Chapter 4

Isolation and characterization of cellulose nanofibre from peel and its application in developing nanopaper

The Chapter 4 has been discussed under two sub-heads as follows:

A) Isolation and characterization of cellulose nanofibers from culinary banana peel using high-intensity ultrasonication combined with chemical treatment

4.1 Introduction

Cellulose the homopolysaccharide representing about $1.5x10^{12}$ tons of total annual biomass production composed of glucose-glucose linkages (β-1,4-linked-glucopyranose unit) arranged in linear chains where C-1 of every glucose unit is bonded to C-4 of the next glucose molecule and nanostructures.[1-3] It is one of the most important biopolymers in existence and is derived from readily available biomass.[4] Due to its availability, biocompatibility, biodegradability and sustainability cellulose is widely used.[5] Cellulose fibers exhibit a unique structure hierarchy derived from their biological origin. They are composed of assemblies of nanofiber diameter ranging 2 to 20 nm and a length of more than a few micrometers. The nanometer sized single fiber of cellulose is commonly referred to as nanocrystals, whiskers, nanowhiskers, microfibrillated cellulose, microfibril aggregates or nanofibers.[5-7] Plants and woods are the primary source of cellulose nanofibers and their compounds encompass current area of research and compared to the commercially available fibers, nanofibers obtained from plant sources poses low density, nonabrasive, combustible, nontoxic, low cost, biodegradable and has good thermal and mechanical properties.[6, 8, 9]

The study of cellulose nanofibers as a reinforcing phase in nanocomposites started almost 15 years ago. Since then, cellulose nanofibers unlock the door in the direction of promising research on cellulose based nano materials with increasing area of potential applications including packaging material,[10,11] transparent material, [12, 13] paper production,[14, 15] and biomedical applications.[16, 17] Cellulose nanofibers could also be used as a rheological modifier in foods, paints, cosmetics and pharmaceutical products.[18] Many studies have been done on isolation and characterization of cellulose nanofibers from various sources like wood fibers,[19] cotton,[20] potato tuber cells,[21] prickly pear fruits,[22] lemon and maize,[23] soybean,[24] wheat straw and soy hulls,[25] coconut husk fibers,[26] branch-barks of mulberry,[27] pineapple leaf fibers,[28] banana rachis,[29] pea hull fiber,[30] and sugar beet.[31] There has been growing interest in researching the

potentiality of using cellulose based nanofibers as a reinforcing material. Cellulose nanofibers can be extracted from the cell walls by chemical and/or mechanical treatment such as cryocrushing,[32] grinding,[19, 33, 34] high pressure homogenization,[35] acid hydrolysis,[36, 37] and biological treatment, like enzyme assisted hydrolysis.[38, 39]

Use of ultrasonic technique for isolation of cellulose nanofibers is an emerging method and has been extensively used by various researchers.[5, 40-42] During the process of ultrasonic treatment ultrasound energy is transferred to cellulose chains through a process called cavitation, which refers to the formation, growth, and violent collapse of cavities in water.[5] The energy provided by cavitation in this so-called sonochemistry is approximately 10-100 kJ/mol, which is within the hydrogen bond energy scale.[43] Thus, the ultrasonic impact can gradually disintegrate the micron-sized cellulose fibers into nanofibers.

In the process of development of value added food products from culinary banana, the peel is a waste material of various fruit and vegetables processing units located in Northeast India. Therefore it is possible to obtain banana peel sufficiently and application depends on its chemical compositions.[44] Literature revealed hitherto unexploited of this biomaterial in terms of its value addition and has enormous potential for its industrial use. Hence the use of this biomaterial will not only help in increasing value addition but also help the environment from pollution free. Knowing the fact that, peel of culinary banana is an abundant source of cellulose, it can be considered as a potential candidate for development of reinforcing composites. As mentioned earlier many researchers have reported their work on cellulose nanofibers from different sources; however, there is hardly any work reported on cellulose nanofibers from culinary banana peel. In the light of the above stated reasons, the aim of this present study was to add value to culinary banana peel by isolating its cellulose nanofibers using chemical treatment followed by high-intensity ultrasonication. The developed material can be used as a reinforcement material in high performance biocomposites and also it will help the environment to be waste free.

4.2 Materials and methods

4.2.1 Raw materials and chemicals

Fresh culinary bananas (*kachkal*) at mature edible stage were collected from Tezpur University campus, Assam. The samples were cleaned thoroughly with running tap water followed by soaking in double distilled water for 1 h to remove any dust or dirt adhering to the peel surface and finally they were wiped with tissue papers and peel flour was prepared. All chemicals used in the present study viz. acetic acid (CH_3COOH), sodium hydroxide (NaOH), potassium hydroxide (KOH), potassium metabisulphite ($K_2S_2O_5$), sodium chlorite ($NaClO_2$), anthraquinone ($C_{14}H_8O_2$), sulfuric acid (H_2SO_4) were analytical reagent grade and procured form HiMedia laboratories, India.

4.2.2 Preparation of peel flour

Previously cleaned culinary bananas were now peeled manually and pulp was separated from peel. The peels were then immediately dipped in solution of 1% potassium metabisulphite for 12 h to inhibit oxidation and enzymatic browning. Subsequently the peels were dried at 50^{o}C for 24 h by using convective tray dryer (Model No. IK-112, Make IKON Instruments, Delhi). The dried peels were ground and passed through 0.25 mm mesh screen, packed in polyethylene bags and stored at 4^{o}C.

4.2.3 Isolation of cellulose fibers (CFs) and cellulose nanofibers (CNFs)

The culinary banana peel flour (yield was 63.35%) having moisture content (6.7%), cellulose (16.62%), hemicelluloses (7.34%), lignin (4.01%) was given first alkali treatment by cooking in a digester (KelPlus, Pelican Equipment, India) with a solution of 20% (w/v) sodium hydroxide and 0.1% anthraquinone with peel flour to solution ratio (1:20) at 170^{o}C for 1.5 h which partially solubilized pectin, lignin and hemicelluloses. The digested peel was washed with distilled water to remove those pectin, lignin and hemicelluloses. The insoluble pellets remained after the first alkali treatment was further delignified with 1% (w/v) sodium chlorite (at pH 5

adjusted with 10% v/v acetic acid) at 70^{o}C for 1 h. The insoluble pellets remained after first bleaching treatment was washed and second bleaching treatment was given again maintaining the same condition as in the first bleaching process which resulted in further effective discolouration and confirming the leaching out of phenolic compounds and lignins. The neutralized insoluble pellets remained after second bleaching process were subjected to second alkali treatment with 5% (w/v) KOH solution at ambient temperature (25±2^{o}C) for 15 h followed by washing which helped in elimination of residual hemicelluloses. Finally, the insoluble pellets were given to acid hydrolysis treatment with solution of 1% (v/v) sulfuric acid at 80^{o}C for 1 h. The acid hydrolysis treatments helped in leaching out traces of minerals, residual starch and also hydrolyzed amorphous cellulose and eased in getting the required nanofibers. After each step of chemical treatment, the insoluble pellets were washed with double distilled water and centrifuged at 10,000 rpm at 4^{o}C for 20 min until the pellets were neutralized. The pellets were kept in water-swollen state during whole chemical process in order to avoid generating strong hydrogen bonding among nanofibers.

The chemically purified cellulose fibers were soaked in deionised water (concentration ~0.5% mass) and subjected to tailoring and size reduction by giving high-intensity ultrasonic treatment. The solution of chemically purified cellulose fibers (120 ml) was placed in ultrasonic generator (UW 2070, Bandelin sonoplus, Germany) having 1.5 cm (diameter) cylindrical titanium alloy probe tip at frequency of 25 kHz. Ultrasonication was carried out for 30 min in order to isolate the cellulose nanofibers. The output power of ultrasonication was conducted at 400, 800 and 1000W individually to characterize the effect of ultrasonic intensity on nanofibrillation of chemically purified cellulose. The ultrasonic treatment was carried out in ice water bath and ice was maintained throughout the sonication time. The detailed steps followed to obtain cellulose nanofibers are illustrated in Fig. 4.1. The obtained nanofibers were freeze dried (LDF 5512, Daihan Labtech Co., South Korea) and stored at 4^{o}C in sealed containers.

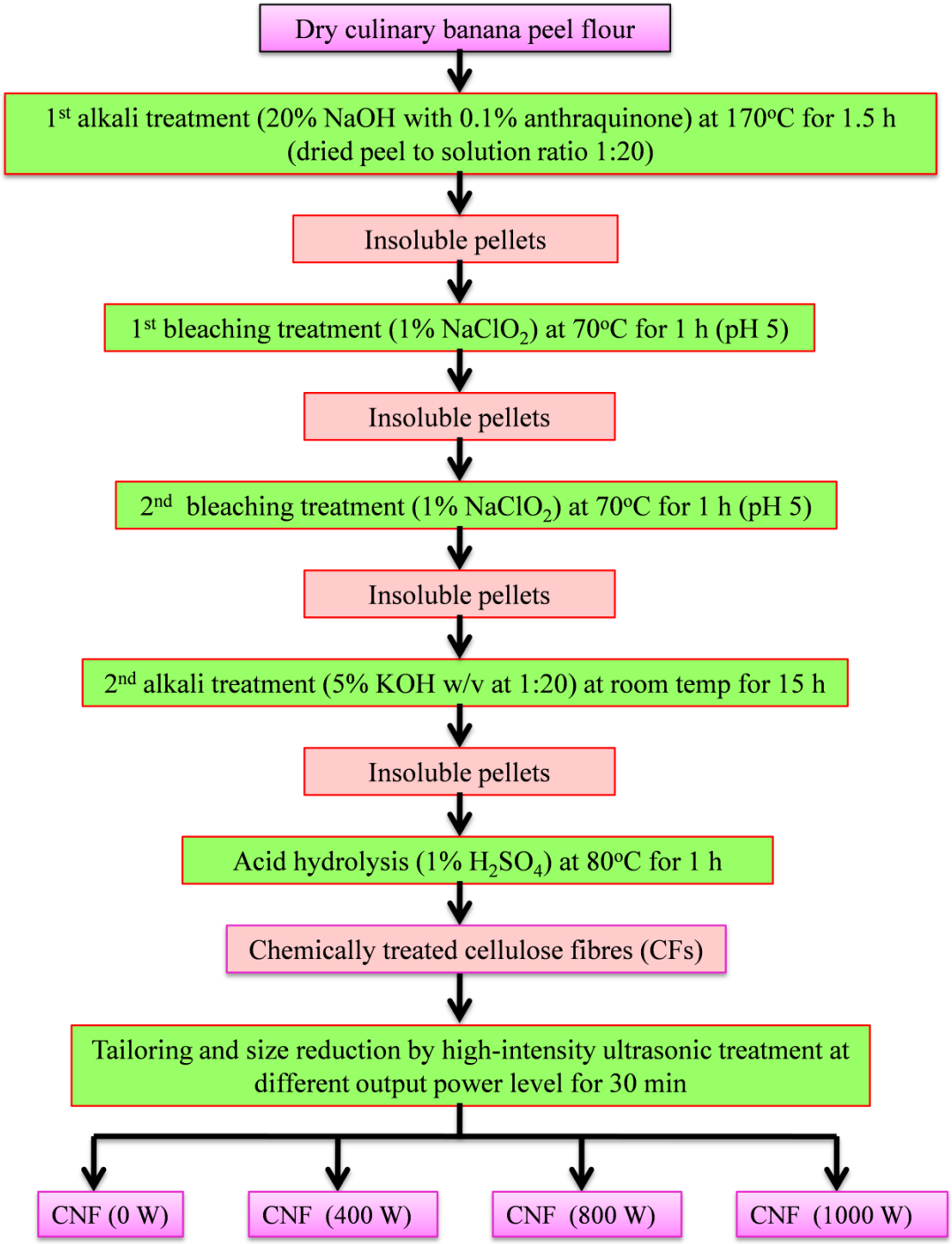

Fig. 4.1 Detailed flow chart for the steps involved in chemical and ultrasonication treatments

4.2.4 Characterization of cellulose nanofibers (CNFs)

4.2.4.1 Microstructure evaluation by scanning electron microscopy (SEM)

Scanning electron microscope (JEOL JSM-6390LV, SEM, Oxford) was used to investigate the microstructure of CNFs obtained after undergoing different chemical and ultrasonic treatments. Samples were placed in a metal stud using double sided tape and coated with a fine layer of gold using a sputter gold coater. Sample micrographs were observed at a magnification of 1000X (scale bar 10 μm) at an accelerating voltage of 20 kV.

4.2.4.2 Transmission electron microscopy (TEM)

The morphology of CNFs was evaluated using TEM (JEM-2100, JEOL, USA). The samples were dispersed by placing them in sonicator for 5 min. Drops of dilute CNFs suspensions were deposited on glow-discharged thin carbon-coated TEM microgrids. The excess liquid was absorbed using filter paper and allowed to dry at ambient temperature. After the specimen was completely dried TEM images was observed at 14,000X (scale bar 2,000 nm) at an accelerating voltage of 80kV. The diameters of CNFs were calculated from TEM images using microscope image analysis system which helped to illustrate size distribution.

4.2.4.3 X-ray diffraction (XRD)

The powder X-ray diffraction patterns were measured using a Rigaku Miniflex instrument at ambient temperature using CuKα radiation (λ = 0.15418 nm) over the 2θ range of 5 and 50° with a scanning speed of 1.2°/min. The CNFs were vacuum dried at 60 °C before the assay. The crystallinity index (I_c) of CNFs was calculated using Segal method (Eq. 4.1).

$$I_c = \frac{I_{002} - I_{am}}{I_{002}} \times 100 \qquad \text{Eq. (4.1)}$$

Where, I_{002} is the diffraction intensity close to 2θ = 22° and represents a crystalline material and I_{am} is the diffraction intensity close to 2θ = 18° referring amorphous material in CNFs.

4.2.4.4 Fourier transform infrared spectroscopy (FT-IR)

IR spectra of CNFs were measured using KBr disk (ultra thin pellets) method. The dry sample was ground and blended with KBr in a ratio of sample/KBr 1:4. The blend was pressed to obtain a pellet and introduced in the spectrometer (Nicolet Instruments 410 FTIR equipped with KBr optics and a DTGS detector, Thermo Scientific, USA). Each spectrum was analyzed in the range of resolution from 400- 4000 cm^{-1} with a resolution of 4 cm^{-1} and total of 64 scans were collected.

4.2.4.5 Thermogravimetric analysis (TGA)

Thermal degradation behavior of CNFs was evaluated using TGA (Shimadzu, TGA-50, North America). The thermal stability of each CNF was conducted at 25 to 600 ^{o}C with constant heating rate of 10 ^{o}C/min under nitrogen atmosphere.

4.3 Results and discussion

4.3.1 Visual examination on appearance of CNFs suspensions

The effect of each chemical treatment given to culinary banana peel flour during the isolation of CNFs was prominently visible. The detailed steps involved during the whole process and change in colour of peel flour in each step due to leaching out of lignin, tannin, pectin, hemicelluloses, proteins, starch, minerals etc are illustrated in Fig. 4.2a. The initial colour of peel flour was dark brown (first alkali treatment) which was changed to light brown (first bleaching treatment) and the gradual discolouration from brown to pure white continued during second bleaching, second alkali and acid hydrolysis steps. The alkali treatment hydrolyzed and solubilized pectins, starch, hemicelluloses, proteins,[45] while bleaching process was employed to remove lignin and tannin which are responsible for the brown colour of peel flour.[35] The bleaching treatment given with 1% $NaClO_2$ solution (pH 5) at 70^{o}C for 1 h helped in bleaching of most of the lignins. As chlorine and chlorites rapidly oxidize lignin and generates hydroxyl, carboxyl and carbonyl groups which facilitate lignin to solublize in alkali medium and the

purification of cellulose took place.[45] Removal of lignin from plant sources using $NaClO_2$ is the most widespread technique used in laboratory.[35] The visual examination to distinguish the changes in colour of peel flour with advancement in chemical treatment has been depicted in Fig. 4.2b

After the chemical treatment, the chemically purified cellulose (CFs) was further given high-intensity ultrasonication treatment in order to tailor and reduce the size of nanofibers. After 30 min of ultrasonic treatment with an output power of 400, 800 and 1000 W, three sets of CNFs were obtained and coded as 400W, 800W and 1000W and suspension 0W was considered as nanofiber without ultrasonic treatment. After ultrasonic treatment a substantial increase in the dispersion of nanofiber suspension was observed when the ultrasonic output power was increased from 400 to 1000W. It was observed that CNFs were not homogenously dispersed in water at 400W and there was a noticeable improvement when the output power increased to 800W. Similarly, the CNFs sufficiently dispersed and became highly viscous suspension with increase in ultrasonic power. This is because high-intensity ultrasonic waves can produce a very strong mechanical oscillating power because of cavitation. The cavitation includes the formation, expansion, and implosion of microscopic gas bubbles when the molecules in a liquid absorb ultrasonic energy. Within the cavitation bubbles and the immediate surrounding area, violent shock waves are produced, which can be used to isolate fibrils from cellulose fibers.[5, 42] The yield of purified cellulose fibres (CFs) was 8.9% (d.b.). Production of good quality CNFs was reliable when chemical and ultrasonic treatments employed one after another.

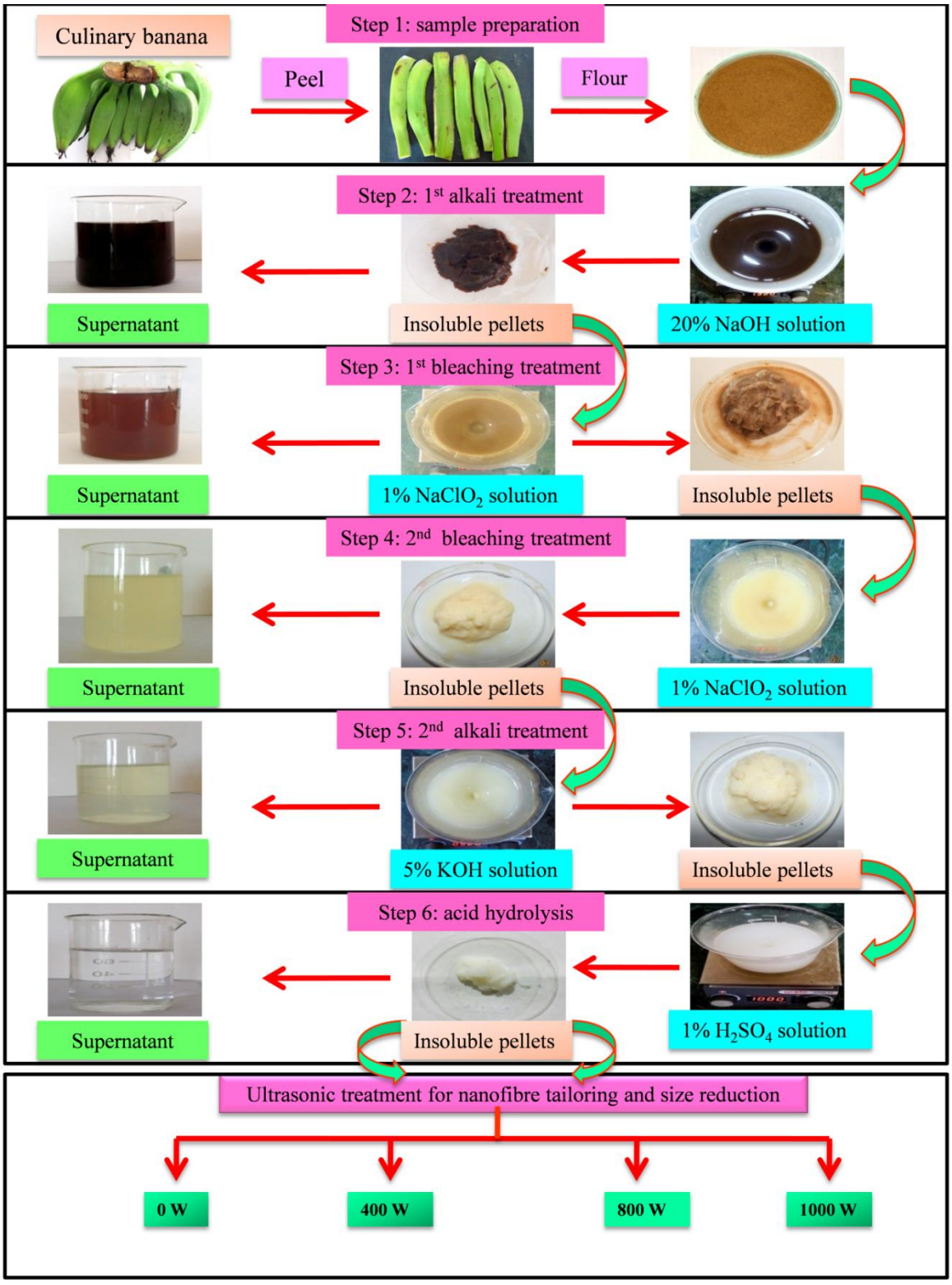

Fig. 4.2a Procedure showing gradual discolouration in peel flour occurred during isolation of CNFs

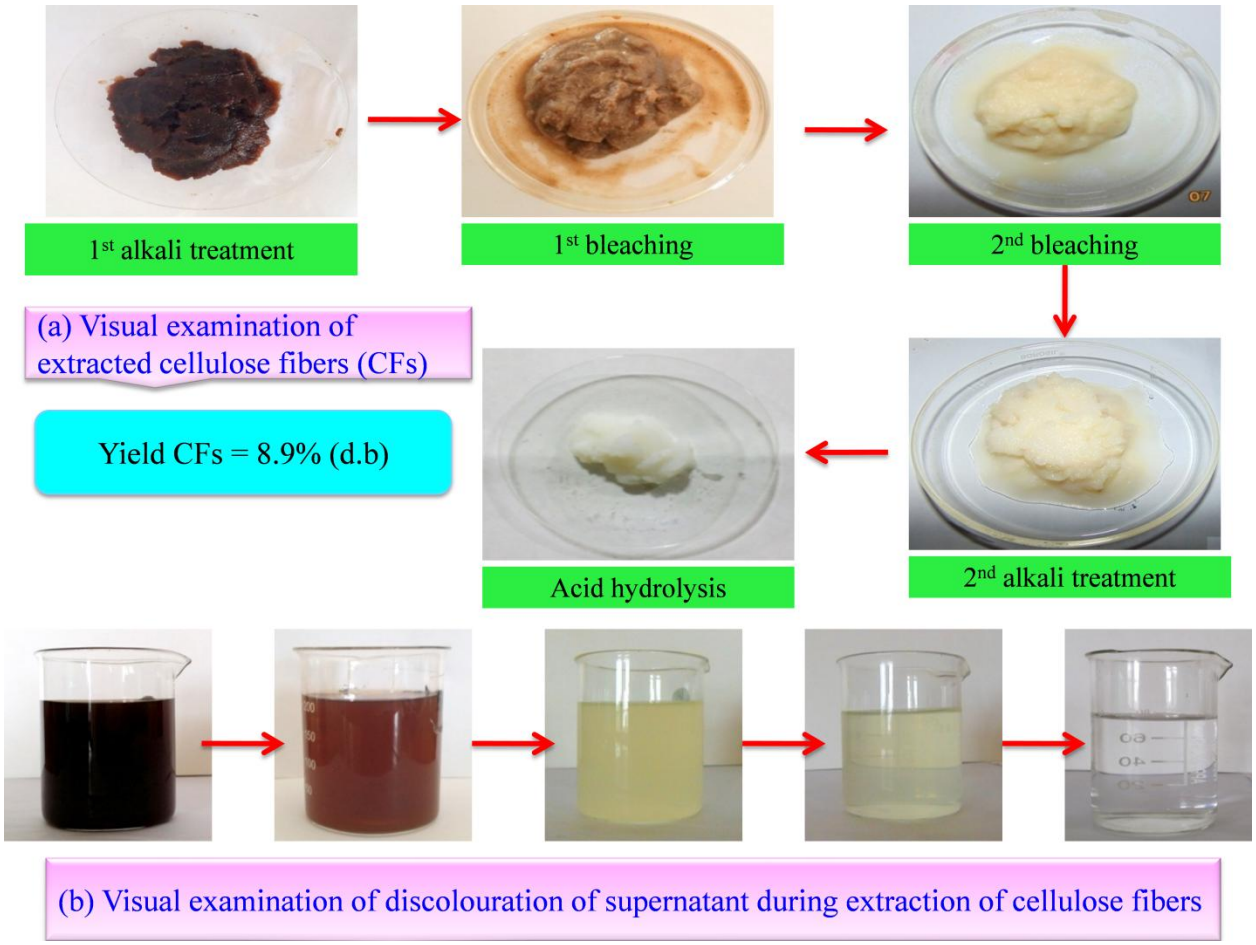

Fig. 4.2b Visual examination on colour change in culinary banana peel flour with advancement in chemical treatment

4.3.2 Microstructure evaluation by scanning electron microscopy (SEM)

The evaluation in the changes of the structure of cellulose nanofibers were evaluated after subjecting to chemical and ultrasonication treatments. SEM images of nanofibers (Figs. 4.3b, 4.3c, 4.3d, 4.3e) were compared with micrographs of culinary banana peel (Fig. 4.3a) which helped to elucidate the structure of these fibers. The microstructure of culinary banana peel showed irregular structure with presence of some starch granules. The chemical treatment helped in removal of amorphous components like lignin, pectin, hemicelluloses.[35] It is evident that chemical treatment employed in bleaching process as well as ultrasonic treatment given for fragmentation (Figs. 4.3b, 4.3c, 4.3d, 4.3e) of obtained nanofibers reduced the chemical and structural changes in the nanofibers. The ultrasonic treatment given to tailor and reduce the size

of nanofibers illustrated a visible fragmentation and tailoring of the nanofibers with respect to treatment given which has been further confirmed by TEM analyses. The plant fibers are complicated multilayered structure because of the interfibrillar hydrogen bonds[46] and the fibers are 'aggregated nanofibers' with a wide distribution in its width.[41]

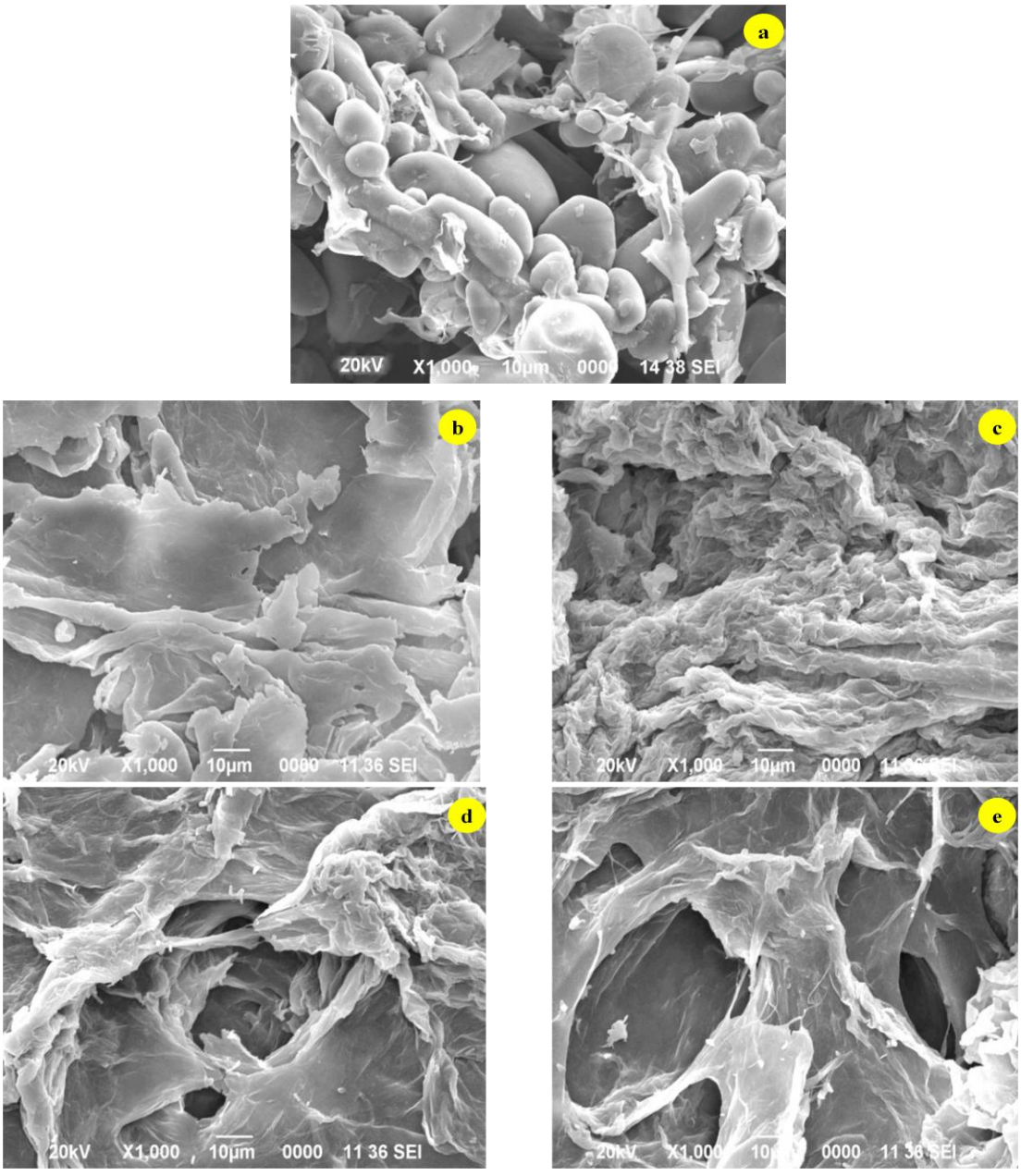

Fig. 4.3 SEM micrographs of **(a)** culinary banana peel and **(b, c, d, e)** cellulose nanofibers obtained by ultrasonic treatment at 0W, 400W, 800W and 1000W respectively

4.3.3 Transmission electron microscopy (TEM)

TEM images of cellulose nanofibers obtained after a 30 min high-intensity ultrasonication treatment at various power levels confirmed the presence of nanofibers (Figs. 4.4a, 4.4b, 4.4c, 4.4d). It could be seen that the chemical treatment eradicated all the amorphous compounds (lignin, pectin, hemicelluloses) and only needle-like cellulose nanofibers were present. The ultrasonic treatment at the output power level of 400W gave large aggregates consisting of wire-like cellulose fibers with number of branches of smaller bundles or partly individualized nanofibers attached. Application of high-intensity ultrasonication treatment evinced neatly fragmented needle like CNFs from chemically purified CFs of culinary banana peel (Table 4.1). Chemical and enzyme assisted hydrolysis were studied by Tibolla, et al.[38] for isolation of CNFs from banana (*Musa paradisica*) peel and TEM results showed chemical treatment was superior over enzymatic treatment. In the present study the CNFs were neatly fragmented needle like when employed high-intensity ultrasonication treatment over the chemical and enzymatic methods employed by the preceding authors. The methods used in the present study are very simple and cost effective compared to chemical and enzymatic treatments as described by earlier workers and in addition it is reliable and has good reproducibility. Literatures revealed that chemical treatment followed by high-intensity ultrasonication is perhaps the first attempt in developing CNFs from culinary banana peel.

Table 4.1 Particle size distribution of cellulose nanofibers (CNFs) observed by TEM

Sample	Diameter, D (nm)	Length, L (nm)	Aspect ratio (L/D)
0W	35 ± 9.5	589.05 ± 3.4	16.83± 5.98
400W	32 ± 7.3	468.87 ± 6.3	14.65± 6.65
800W	27 ± 6.6	384.9 ± 5.3	14.25± 6.02
1000W	20 ± 5.2	263.9 ± 7.2	13.19± 6.11

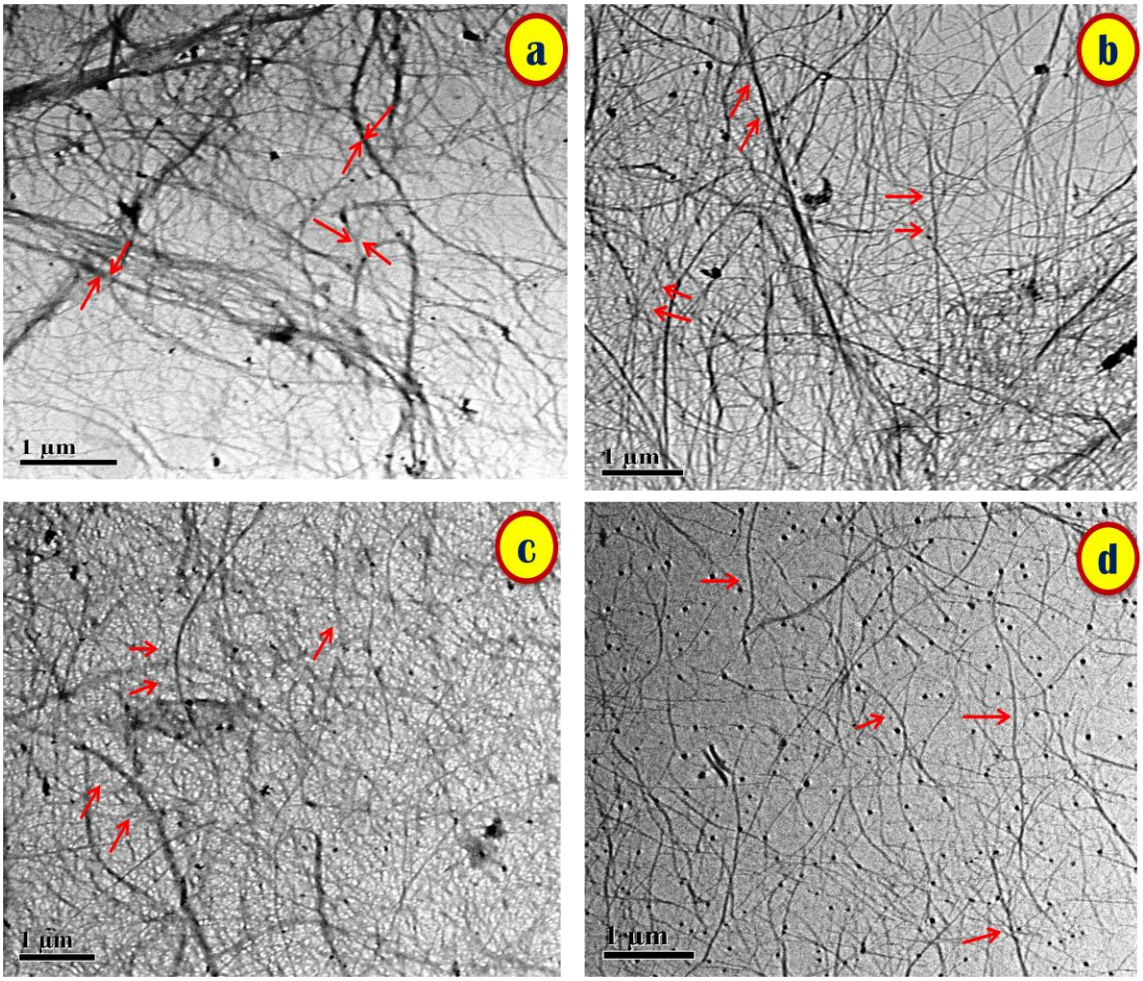

Fig. 4.4 TEM images of cellulose nanofibers obtained at various ultrasonic treatment **(a)** 0 W, **(b)** 400 W, **(c)** 800 W and **(d)** 1000 W

4.3.4 X-ray diffraction (XRD)

The crystallinity of cellulose is an important factor for determining its thermal and mechanical properties. In the present study the x-ray diffraction pattern of cellulose nanofibers from culinary banana peel obtained by various ultrasonic treatments (0W, 400W, 800W and 1000W) were investigated. The XRD graphs (Fig. 4.5) clearly revealed that all difractrograms exhibit sharp peaks at $2\theta = 16^{o}$ and $2\theta = 22^{o}$, which represented typical cellulose I form indicating higher crystallinity of nanofibers (Rosa et al., 2010). The result indicated that during the chemical as well as ultrasonic treatments, the crystalline structure of culinary banana peel cellulose did not change. The crystallinity index (I_c) calculated using Eq. (4.1) was 30.50%,

44.14%, 50.74% and 63.64% for 0 W, 400 W, 800 W and 1000 W respectively. High-intensity ultrasonication output power level influenced the homogenization and fragmentation on the crystalline nature of CNFs and crystallinity increased gradually with increase in output power (0-1000W). This clearly showed that higher output power levels given for homogenization removed part of amorphous portion of CNFs. The result has also been favourably supported by the FT-IR analysis. Chen et al.[5] also reported similar findings on cellulose nanofibers from wood.

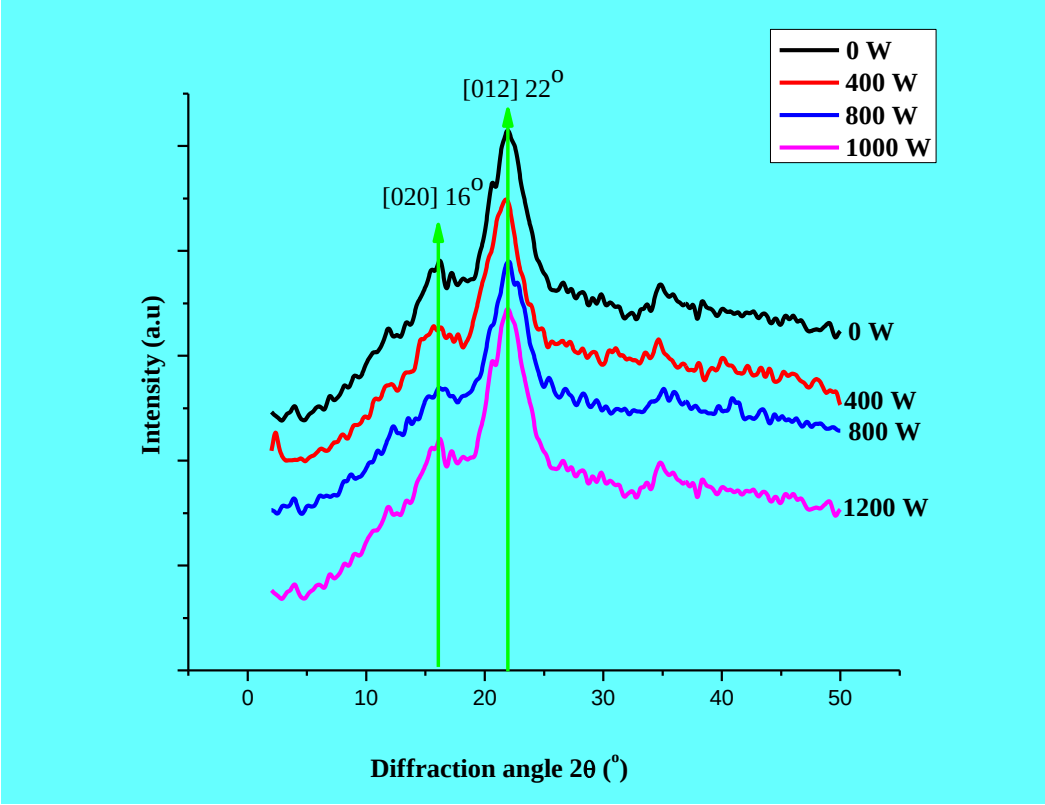

Fig 4.5 XRD diffraction pattern of cellulose nanofibers from culinary banana peel

4.3.5 Fourier transform infrared spectroscopy (FT-IR)

The Fourier-transform infrared spectroscopy is a suitable technique to ascertain the vibrations or stretch caused by different treatments on the chemical structure of the isolated samples. The FT-IR spectra of culinary banana peel cellulose nanofibers are elucidated in Fig. 4.6 where similar spectral patterns were noticed in all the samples. In the region of 3000-3650 cm^{-1} the broadened absorption band distinctive to the –OH stretching was observed in all spectra.

The band observed at 3442 cm^{-1} corresponds to intramolecular hydrogen bonding in cellulose II.[47] At 2914 cm^{-1} a small peak was observed which can be attributed to the aliphatic saturated C-H stretching vibration in cellulose and hemicelluloses,[35] further it may also be considered that waxes were eliminated after the various chemical treatments.[48, 49] The shoulder at 1732 cm^{-1} which is almost absent in all the spectra is attributed to vibrations of acetyl and uronic ester groups of hemicelluloses or ester linkage of carboxylic group of the ferulic and p-coumaric acids of lignin and/or hemicelluloses.[29] This may be attributed to the chemical treatment which dissolved hemicelluloses and lignin components present in the sample. The prominent band at 1635 cm^{-1} represented the bending mode of the absorbed water.[50] According to the FT-IR studies of Pelissari et al.[35] and Wang et al.[51] usually in the banana peel at around 1608-1640 cm^{-1} bands are often visible and was not traced in the present study and may be due to the partial reaction of the C=O bonds of hemicelluloses and was bleached during chemical treatment of cellulose nanofibers. Indeed the vibration at 1233 cm^{-1} can be represented as guaiacyl ring with stretching C=O. At 1554 and 1375 cm^{-1} two peaks were observed which indicated aromatic C=C stretch from aromatic ring vibration of lignin. The prominent band of C-O-C pyranose ring skeletal vibration stretching at 1030 cm^{-1} was observed in all the four spectra. It indicates presence of xylans are associated with hemicelluloses which confirmed that xyloglucans are strongly bound to cellulose nanofibers also the intense band at this wavenumber proves higher cellulose content in chemically treated cellulose nanofibers.[29, 48,49] A less intense band at 920 cm^{-1} can be attributed to the C-O stretching which seems to be dissolved during the chemical treatment process.[52] At 850 cm^{-1} a sharp band was observed in all the spectra of cellulose nanofiber samples which represented the typical structure of cellulose. It is attributed to glycosidic C-H deformation with the ring vibration of O-H bending and confirms presence of β-glycosidic linkages between the anhydroglucose units of cellulose.[53]

4.3.6 Thermogravimetric analysis (TGA)

The thermogravimetric analysis curve for cellulose nanofibers are illustrated in Fig. 4.7. The TGA curve showed an initial weight loss in the region of 25-150^{o}C which is due to the evaporation of moisture and initial thermal decomposition. The thermal stability of nanofibers slightly decreased according to the partial dissolution process which may be accredited to

reduction in apparent crystallinity.[54] The initial degradation temperature for 0W, 400W, 800W and 1000W was initiated at 260.81°C, 270.41°C, 279.87°C and 295.33°C respectively. The decomposition temperature of all cellulose nanofibers under various ultrasonic treatment levels had little effect on thermal decomposition of cellulose. The glycosidic linkage of cellulose broke down due to depolymerization of hemicelluloses in the region ranging from 220-300°C.[55] In all the samples the broad peak at 220-400 °C is attributed to cellulose degradation.[35] The results of TGA can be corroborated with XRD and FT-IR outcome, indicating that ultrasonic process did not influence chemical composition, crystal structure and thermal stability but only structural changes occurred apparently. Our findings are in line with the results of cellulose nanofibers from wood reported by Chen et al.[5] The main application of cellulose nanofibers in the nanocomposite field is primarily as a reinforcing agent and biocomposite processing, wherein the processing temperature for thermoplastic polymer rises above 200°C.[56] Thus the high thermal stability of cellulose nanofibers from culinary banana peel can serve the purpose as an effective reinforcing material which can be used in food packaging. A further study will be carried out with application of these CNFs in the field of biodegradable composites.

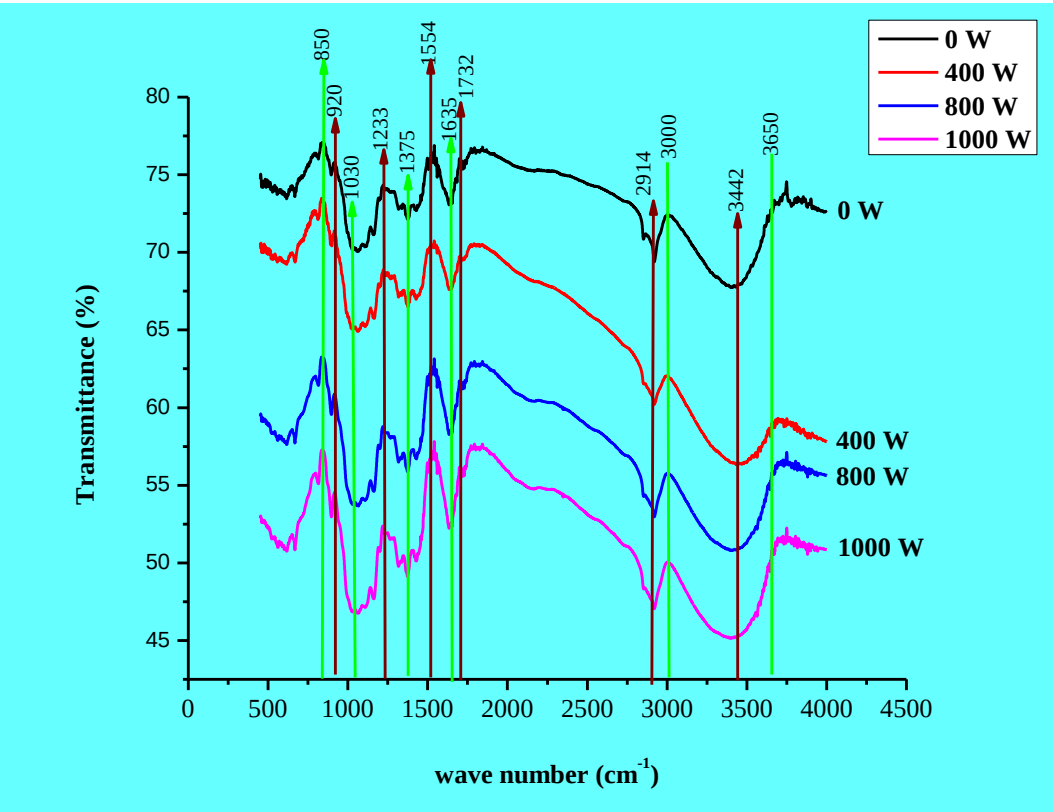

Fig. 4.6 FTIR spectra of cellulose nanofibers from culinary banana peel

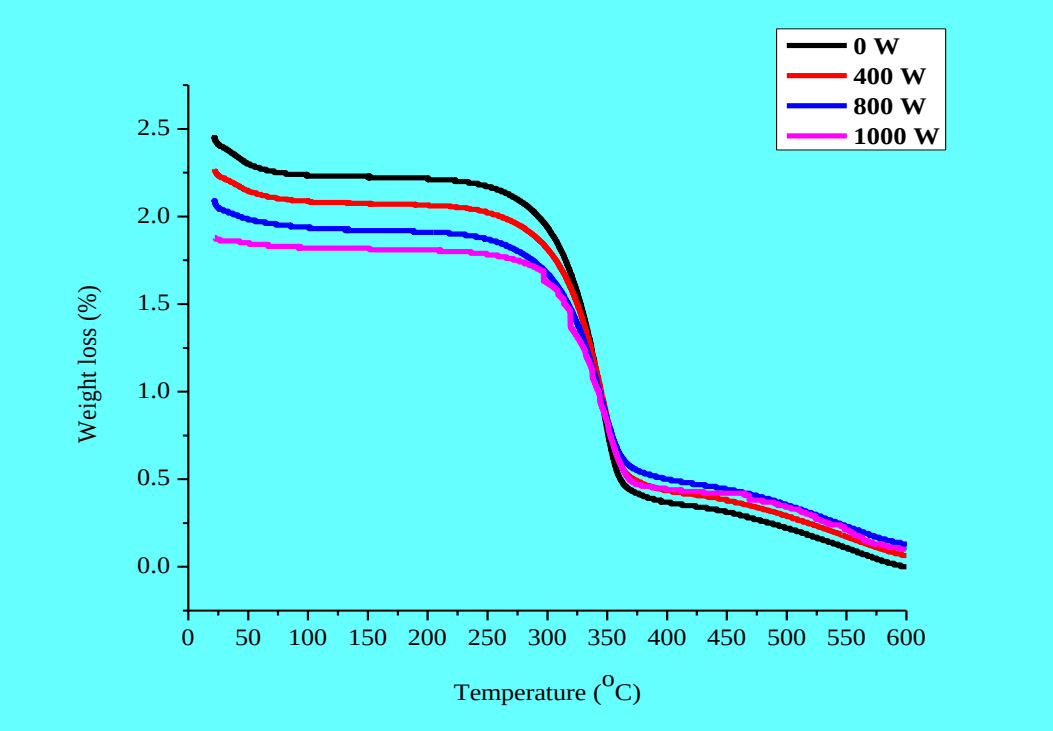

Fig. 4.7 TGA curve of cellulose nanofibers from culinary banana peel

4.4 Conclusion

The present work revealed that culinary banana peel is an interesting source of biomaterial for the production of CNFs. Chemically purified cellulose was isolated using chemical treatment (alkali, bleaching and acid hydrolysis) followed by individualization of CNFs using high-intensity ultrasonication at various output power levels which helped in homogenization, tailoring and size reduction of each CNFs. TEM microstructure confirmed the presence of nanofibres. The CNFs got reduced with the gradual increase in the output power of ultrasonic treatment. The SEM microstructure and FT-IR measurements exemplified that treatments employed, substantially removed hemicelluloses, lignin and other non-cellulosic compounds. All the diffractograms of XRD exhibited sharp peaks at $2\theta = 16^{o}$ and $2\theta = 22^{o}$, which illustrated typical cellulose I form, indicating higher crystallinity of nanofibers. The CNFs also exhibited enhanced thermal properties and stability that increased from 260.81^{o}C to 295.33^{o}C when the output power of ultrasonication treatment increased from 0-1000 W. In the present study, results of chemical treatment followed by high-intensity ultrasonication

favourably justified the production of CNFs from culinary banana peel. It has huge application as a reinforcement agent for the manufacture of bionanocomposites and can be considered as a renewable source of nanofibres which has an etymology to agro-waste.

B) Production of renewable high performance cellulose nanopaper from culinary banana (*Musa* ABB) peel and its characterization

4.5 Introduction

Rapid advancement in the field of nanotechnology has opened up prospects for cellulose, the most abundant natural polymer on earth. Cellulose has gained more attention in the form of nanocellulose that can be used as advanced and novel biomaterial because of its exceptional advantages like biodegradability, biocompatibility, renewability, economical and chemical stability.[57, 58] Nanocellulose is unique and natural material that can be extracted from native cellulose. The primary sources of nanocellulose are woods and plants and can be produced by defragmentation of cellulose of larger unit (cm) to the smaller unit (nm) with the dimension ranging from 5-20 nm. Cellulose nanofiber, the material containing fibers with its length in micrometer and width in nanometric range having structural hierarchy network encompasses current area of research and contemplated as next generation renewable reinforcement for high performance biocomposites production.[59]

The increasing demand for sustainability of environment is gaining research focus into biodegradable and biocompatible materials with the concept of "Green" materials.[60] In this context, cellulose nanofibers (CNFs) may be considered as an attractive biomaterial. Beside its biodegradable, renewable or biocompatible properties, CNFs are mechanically strong, stiff, and highly crystalline with outstanding thermal stability.[38] CNFs have extensive applications including packaging material and most importantly in paper production .[61]

Cellulose nanopapers (CNP) obtained from CNF is similar to conventional paper but constitutes a network of nanofibers having pore size in the range of nanometer. It possesses excellent mechanical properties with high optical transparence, low thermal expansion and has good oxygen barrier characteristics.[62-64] It has potential to be used as a strong sheet like material as well as light weight reinforcement material in biocomposites. Irimia-Vladu[60] used CNP to replace traditional glass and plastic in energy devices and termed as "Green" electronics to produce eco-friendly electronics by developing new green and efficient routes. CNFs are used in preparation of CNP employing various methods including drying of CNF suspension into continuous rolling process[65], vacuum filtration[66], hot pressing[67], solvent casting,[66] pressure

filtration.[68] The structure of CNP shows tightly packed nanofibers and interacts strongly with each other, contributing outstanding mechanical properties and thus CNP from CNF are considered as green and potential alternative for multiple applications depending on the requirements of final use applications including food packaging.[69] In the present study, culinary banana peel is utilized for developing CNP and detailed investigation on properties of developed nanopaper was carried out in terms of suitability for packaging of foods etc. The characterization of developed CNP for its nanostructure properties was performed by using various techniques viz., SEM, TEM, XRD, FT-IR, solid state high resolution ^{13}C NMR and thermal analysis (TGA/DTG) etc. in addition, photoluminescence, light absorption, tensile properties and particle size distribution of CNP were also evaluated.

4.6 Materials and methods

4.6.1 Raw materials and isolation of CNF

Culinary bananas were collected from Tezpur University campus. Peel flour was obtained as described in (section 4.2.2) and CNF were isolated following the method described in (section 4.2.3)

4.6.2 Preparation of cellulose nanopaper (CNP)

The disintegrated and individualized CNF in completely dispersed form were obtained after ultrasonic treatment and was vacuum filtered (funnel diameter 5 cm) using a nylon membrane filter (0.2μm pore size) and then dried under vacuum at 93^{o}C for 10 min using hot press. The CNP was further activated by dipping sequentially in distilled water, acetone, dimethyl acetamide (DMAc) for 2 h at 25^{o}C. The CNP was again immersed in DMAc/LiCl (8% LiCl) for 1 h. Prior to use, DMAc and LiCl (lithium chloride) were dried in oven at 105^{o}C to avoid any negative effect of water on dissolution of CNF.[54] CNP were then dipped in ethanol for 16 h (ethanol was replaced 10 times to rinse the solvent during this time). The rinse sheets were dried using hot press under vacuum at 93^{o}C for 10 min and finally the fine sheet of CNP was obtained. Two sets of CNP was prepared, the control (coded as CNP-UT) without disintegration

of fibers (without high-intensity ultrasonication treatment) and CNP after undergoing ultrasonication treatment (coded as CNP-T). The CNP measured a thickness of 25 μm with a diameter of 5 cm. The photograph of the steps involved in isolation of CNP is illustrated in Fig. 4.8.

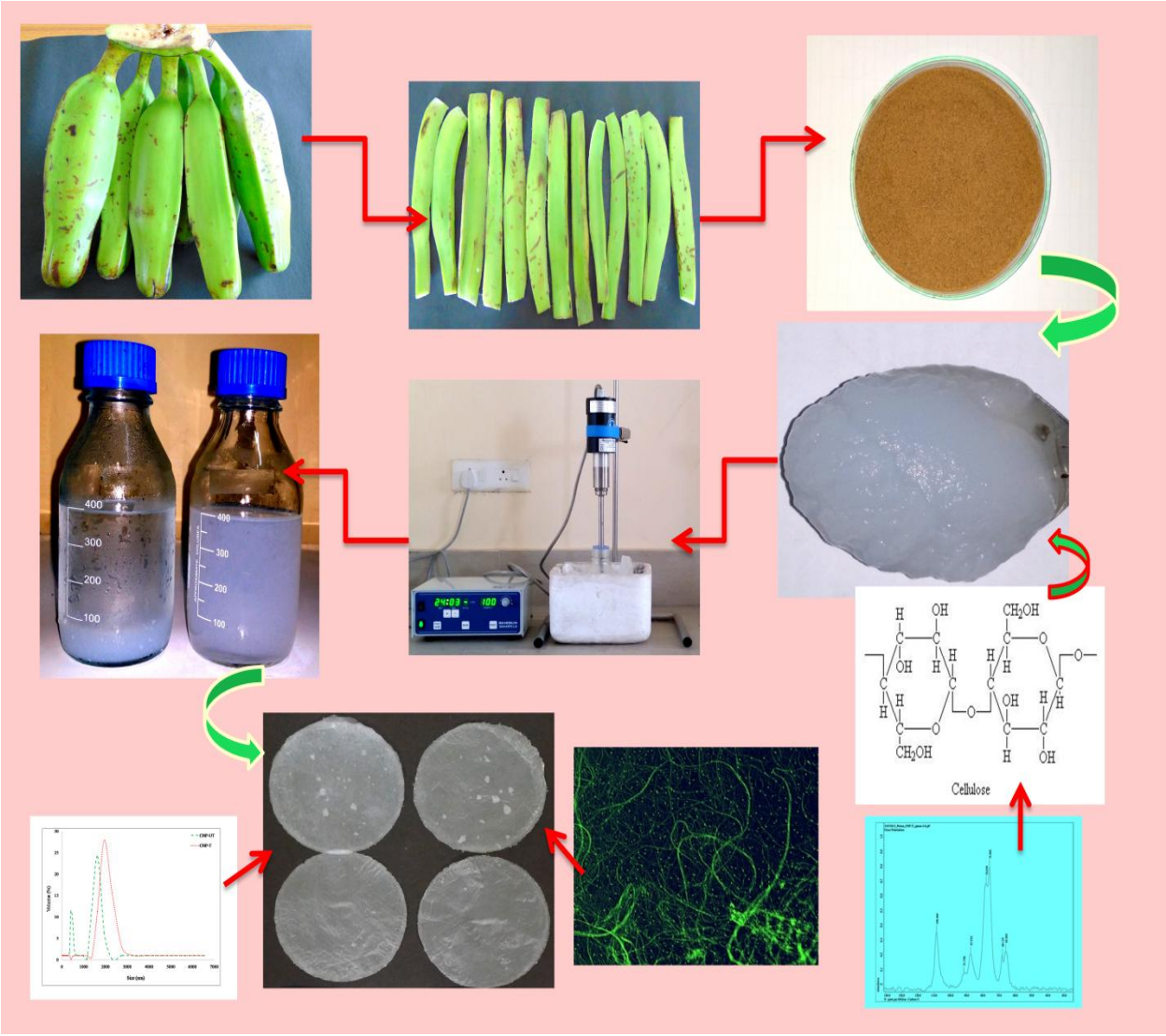

Fig. 4.8 Culinary banana, its peel, flour and cellulose obtained after chemical and ultrasonication treatment and developed CNP

4.6.3 SEM and TEM micrographs of CNP

The microstructure of CNP was evaluated using scanning electron microscope (JEOL JSM-6390LV, SEM, USA) was used as described in (section 4.2.4.1) and TEM images were observed using TEM (JEM-2100, JEOL, USA) (method described in section 4.2.4.2)

4.6.4 X-ray diffraction (XRD)

The powder X-ray diffraction patterns were measured using XRD (Rigaku Miniflex, Japan) as described in (section 4.2.4.3). The crystallinity index (I_c) of CNFs was calculated using Segal method (Eq. 4.1). The crystallite size (D) of the CNP-UT and CNP-T was estimated by Scherrer's Eq. in respect of (200) plane

$$D = \frac{K\lambda}{\beta cos\theta} \quad \text{Eq. (4.2)}$$

Where, K is the correction factor and usually taken to be 0.91, λ is the radiation wavelength of x-ray which is 0.15418 nm, β is the corrected angular width (in radians) or full width at half maxima (FWHM), θ is the diffraction angle (Bragg's angle).

4.6.5 Fourier transform infrared spectroscopy (FT-IR)

Infrared spectra of CNP were measured in spectrometer (Nicolet Instruments 410 FTIR equipped with KBr optics and a DTGS detector, Thermo Scientific, USA) as described in (section 4.2.4.4).

4.6.6 Solid-state ^{13}C nuclear magnetic resonance (NMR) measurements

^{13}C cross polarization magic angle spinning nuclear magnetic resonance (^{13}C CP/MAS-NMR) spectra of CNP were detected using solid state NMR system (JEOL, Japan) at 400MHz with the help of inbuilt DELTA (δ) software (version G4.3.6, Japan) and total of 35 scans were collected.

4.6.7 Thermogravimetric analysis (TGA)

Thermal degradation behavior of CNP was evaluated using TGA and its corresponding derivative DTG (Shimadzu, TGA-50, North America) following the method described in (section 4.2.4.5).

4.6.8 Photoluminescence (PL) and uv-vis spectroscopy

The PL spectrum of 0.1 mg/ml aqueous solution of CNP was evaluated using PL spectrophotometer (model LS 55, PerkinElmer, Singapore PTE Ltd., Singapore) at wavelength range of 500-650 nm with an excitation at 490 nm.[70] The opacity was determined in the range of 200-800 nm using uv-vis spectrophotometer (Shimadzu 1700, Japan).[71]

4.6.9 Mechanical properties

The mechanical properties of CNP were investigated in terms of tensile strength. Universal testing machine (UTM, Zwich Z010, USA) was employed for determination of tensile strength using test standard DIN ISO 1924-3 for papers and boards equipped with 500 N load cell. The CNP were cut into a rectangular strip with a width of 5mm and tensile stress-strain curves were recorded at a strain rate of 10%/min and crosshead speed of 5 mm/min. The thickness of CNP was measured 25μm and the tensile properties are based on the average value of data collected from 7 specimens.[72]

4.6.10 Particle size distribution and zeta potential

The particle size, zeta potential and length size distribution of each nanofiber in CNP were analyzed using particle size distribution and zeta potential analyzer equipped with dynamic light scattering (DLS) system (Microtrac Nanotrac Wave, MN401, USA). Ethanol was used as a solvent in order to improve dispersibility of the sample and dispersion was filtered through 5μm membrane.

4.7 Results and discussion

The chemical treatment given for CNF isolation was effective and in every step of alkali (NaOH and KOH), bleaching ($NaClO_2$) and acid (H_2SO_4) treatment the visible discolouration of peel flour from dark brown to light yellow and finally milky white was observed. Chemical treatment helped in leaching out of hemicelluloses, lignin, pectin, tannin, phenolics, minerals, starch, protein and other non-cellulosic compounds effectively. The solubilize pectin, hemicelluloses, starch, protein etc were hydrolyzed during alkali treatment.[45] and lignin and tannin were bleached by $NaClO_2$.[35] The chlorine and chlorites rapidly oxidize lignin and generates hydroxyl, carboxyl and carbonyl groups which helped lignin to solubilize in alkali medium and the purification of cellulose took place.[45] The traces of minerals, residual starch and amorphous cellulose leached out during acid hydrolysis and finally the required CNF was obtained in the form of white gel like crystals having a yield of 9.21%. The photograph of developed CNP-UT and CNP-T is illustrated in Fig. 4.9.

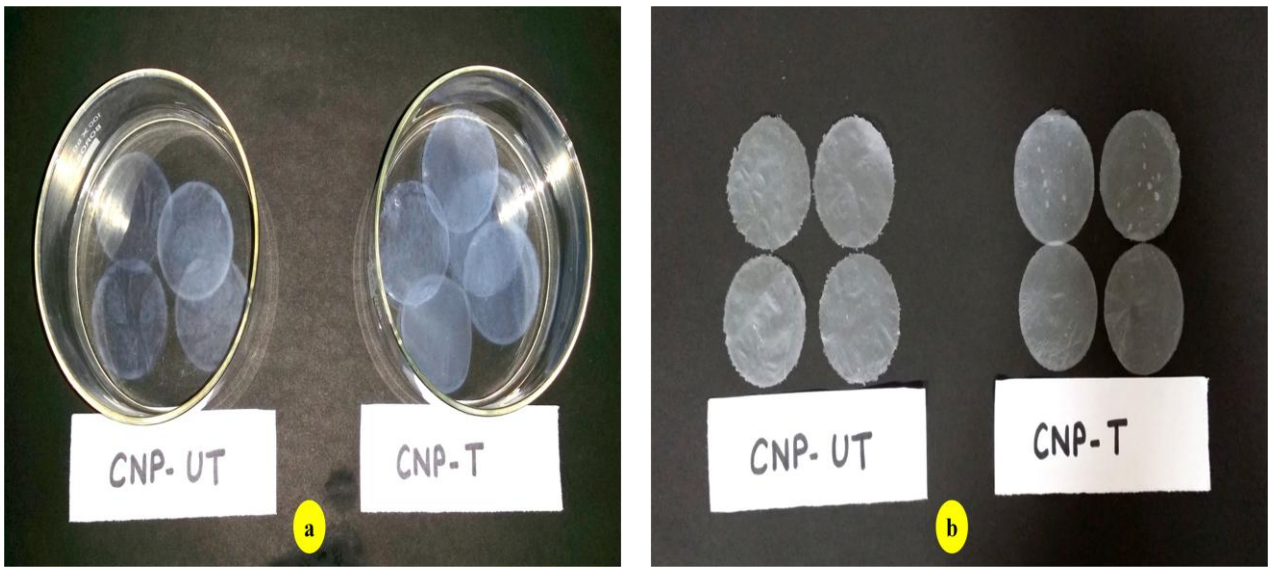

Fig. 4.9 Cellulose nanopaper (CNP) **(a)** during activation period and **(b)** after drying

4.7.1 Structural morphology by SEM

The scanning electron micrographs at Figs. 4.10a and 4.10b illustrate the structural morphology of CNP-UT and CNP-T. The chemical treatments employed for isolation of CNF was extremely effective and amorphous components like lignin, pectin, hemicelluloses were adequately removed.[35] The morphology of CNP-UT (Fig. 4.10a) showed agglomerated structure while CNP-T (Fig. 4.10b) looked more tailoring and fragmentation. The ultrasonic treatment helped in disintegration of CNF into further tailoring and size reduction of individual fibers. One particular area in Fig. 4.10b looked less like a fiber but more like a bunch of tubes and the plausible reason may be the partial formation of nanotubes occurred during chemical and high-intensity ultrasonication treatment. Nanotubes are usually tube shaped hollow material with lesser in diameter than nanofibers, and in the present study partial presence of nanotubes in CNP-T is confirmed by TEM analyses (Fig. 4.11b).

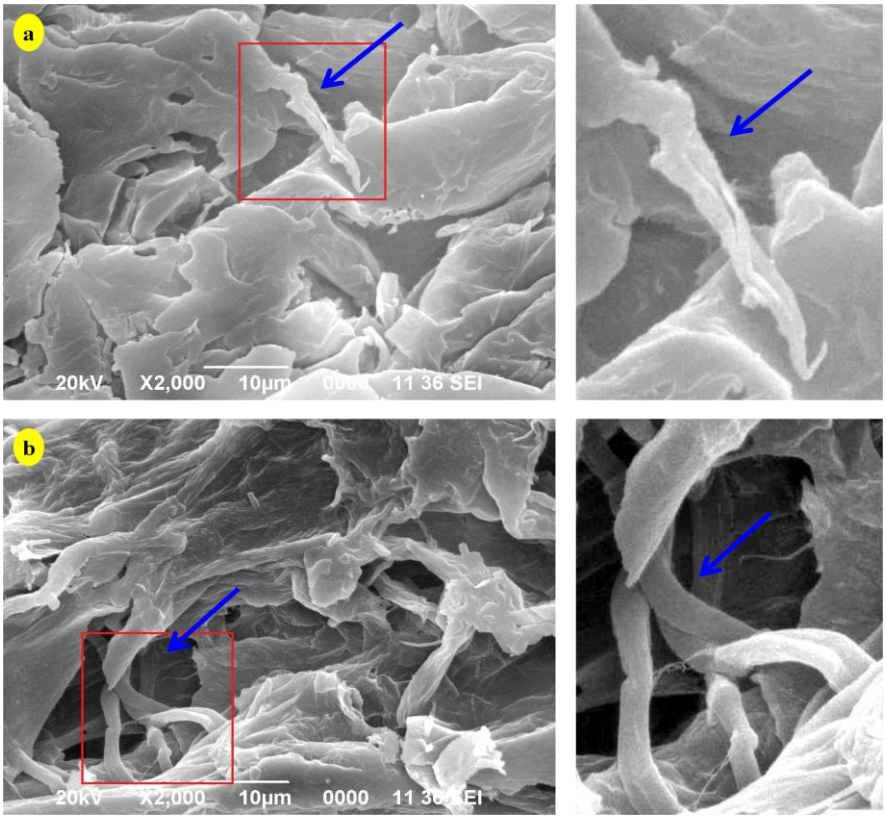

Fig. 4.10 SEM micrographs of **(a**) CNP-UT and **(b)** CNP-T

4.7.2 Nanostructure evaluation by TEM

The nanostructure morphology further studied by TEM revealed that CNP is made up of needle like fine CNF and is arranged in a web like structure (Figs. 4.11a and 4.11b). The TEM micrograph of CNP-UT comprised network of large aggregate of wire-like cellulose fibers with number of branches of smaller bundles or attached with partly individualized nanofibers. The average diameter and length of CNP-UT was found to be 43.76 and 1389.65 nm respectively (Table 4.2). On the other hand, defibrillation of CNF was evident in TEM micrographs of CNP-T. The diameter and length of CNF in CNP-T substantially decreased when high-intensity ultrasonication treatment given. The disintegration and individualization of CNF resulted in smaller and thinner individual fibers with average diameter and length of 10.32 and 536.07 nm respectively. The TEM images (Fig. 4.11b) further evinced a partial formation of hollow, thin and finer round tube shaped structure like nanotubes. The plausible reason behind the formation of nanotubes may be during ultrasonication treatment; ultrasound energy transferred to cellulose chains and generates cavitation bubbles in the solution. The cavitation bubbles collapse to produce shock waves of high temperature and pressure which are known as hotspot and in addition, pyrolysis and radical reaction occurs at hotspot (Chen et al., 2011; Yamada et al., 2010). The energy provided by cavitation in this sonochemistry is approximately 10-100 kJ/mol, which is within the hydrogen bond energy scale.[43] Hence, the ultrasonic impact can gradually synthesize and disintegrate the CNF into nanotube scale and application of ultrasonication treatment in synthesis of nanoparticles to nanotubes has been reported by various authors like.[73, 74]

Table 4.2 Particle size distribution of Cellulose nanopaper (CNP) observed by TEM

Sample	Diameter, D (nm)	Length, L (nm)	Aspect ratio (L/D)	Zeta (ζ)potential (mV)
CNP-UT	43.76±1.34	1389.65±5.67	31.74±1.43	-2.6±0.01
CNP-T	10.32±0.97	536.07±3.44	51.94±2.45	5.4±0.57

Values represent mean± SD, n=3

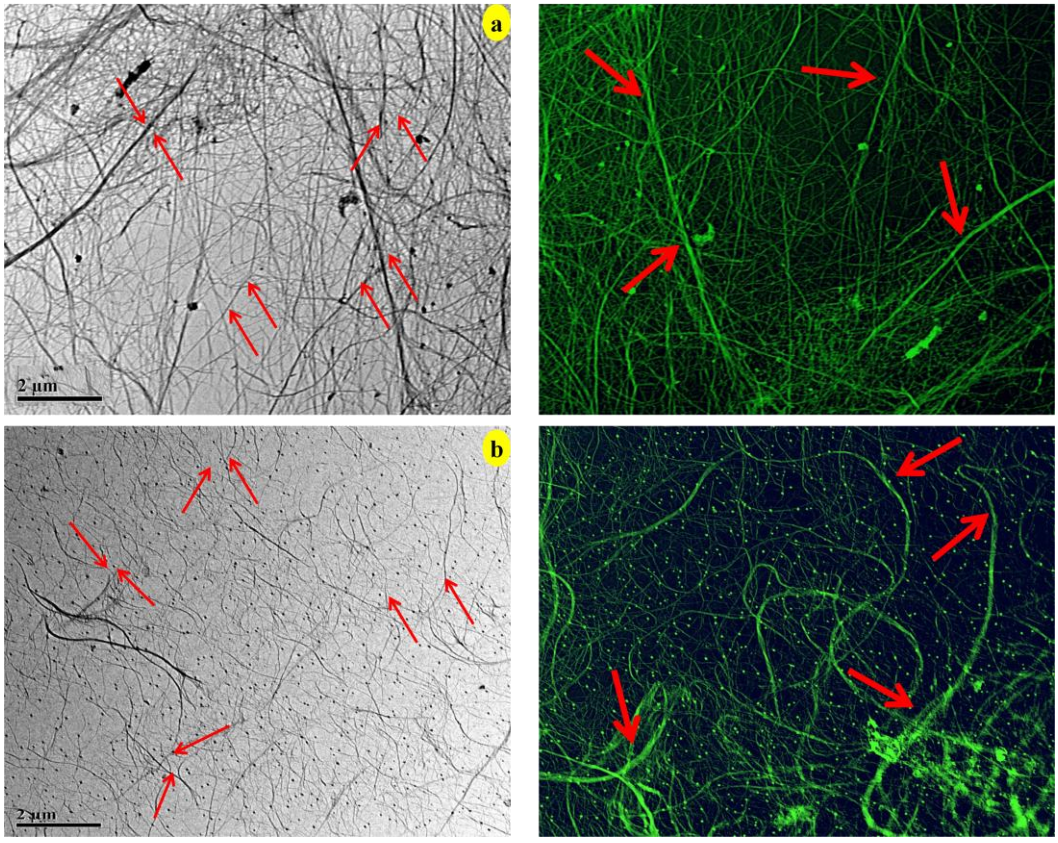

Fig. 4.11 TEM micrographs of **(a)** CNP-UT and **(b)** CNP-T

4.7.3 X-ray diffraction (XRD)

The diffraction spectra used to evaluate the effect of chemical and ultrasonication treatments on crystallinily and crystal type of CNP-UT and CNP-T exhibited typical spectra of cellulose I with three crystalline peaks at around $2\theta = 16^{o}$, 35^{o} and 22^{o} corresponding to the (110), (002) and (004) planes (Fig. 4.12). The chemical treatment employed for isolation of cellulose from peel flour was substantially effective in leaching out all non-cellulosic components. Cellulose has well defined crystalline structure due to its hydrogen bonding and van der Waals forces between adjacent cellulose molecules.[75] The crystallinity index (I_c) of CNP-UT and CNP-T was calculated and found 37.16 and 68.45% respectively (Table 4.3). The higher crystallinity of CNP-T might be attributed to ultrasonication treatment given for homogenization and removed part of amorphous portion of CNF and also associated with higher tensile strength, rigidity and stiffness.[76] The crystallite size measured for CNP-UT and CNP-T was 3.09 and 2.53

nm respectively. The size of individual crystal of CNP-T was smaller compared to CNP-UT and may be attributed to the ultrasonication treatment given for disintegration of fibers. The alkali treatment given during isolation of CNF is believed to increase the stiffness of the fiber by removing other non-cellulosic compounds.[77] On the other hand, during acid hydrolysis treatment the hydronium ion penetrates into amorphous region of cellulose and releases individual crystallites.[78]

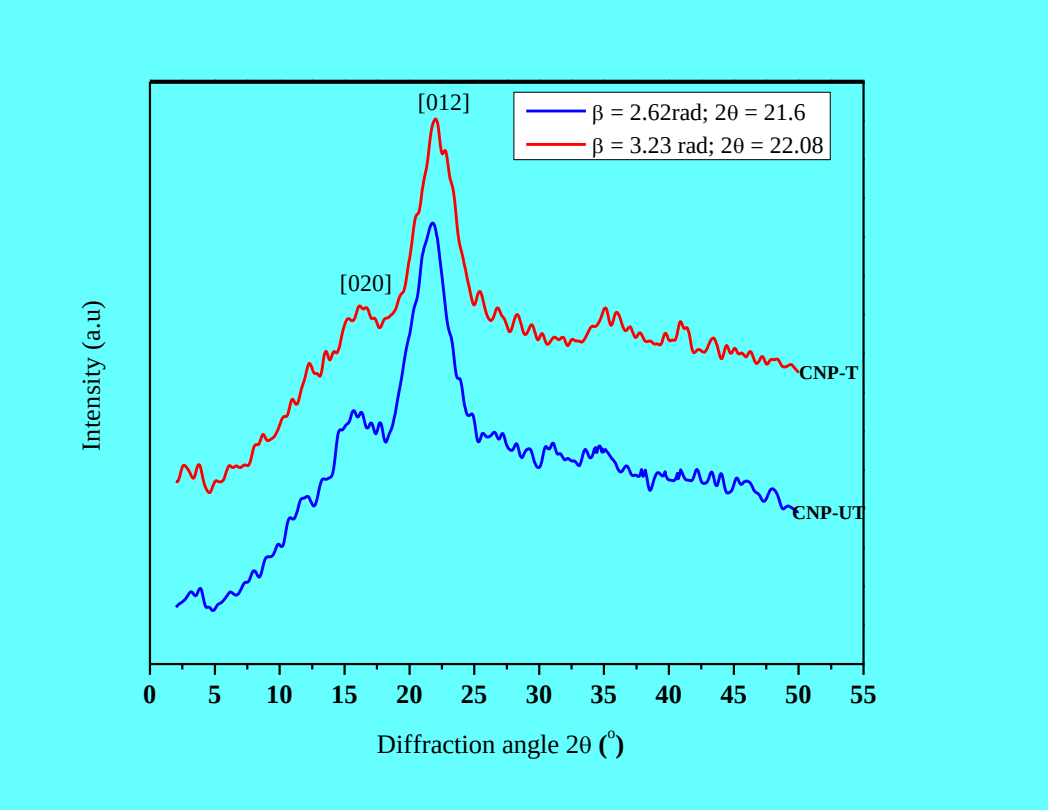

Fig. 4.12 XRD diffraction pattern of CNP-UT and CNP-T

Table 4.3 Crystallinity index and crystallite size of CNP

Sample	Crystallinity index (Ic) (%)	Crystallite size (D) (nm)
CNP-UT	37.16±0.78	3.09±0.04
CNP-T	68.45±1.45	2.53±0.28

Values represent mean± SD, n=3

4.7.4 Fourier transform infrared spectroscopy (FT-IR)

The infrared spectra of CNP-UT and CNP-T were recorded in the range of 400-4000 cm^{-1} (Fig.4.13) and helped in the identification of functional groups present in the sample. A broad spectral band located in the region of 3000-3600 cm^{-1} is attributed to -OH stretching which has emerged from the vibrations of intermolecular hydrogen bonded hydroxyl groups and represents the hydrophilicity of CNP.[38, 75] At 2911 cm^{-1} a band was observed which is due to aliphatic saturated C-H stretching vibration in cellulose and hemicelluloses.[35] This C-H stretching vibration was intense in CNP-T than CNP-UT and it is believed that waxes were eliminated completely in CNP-T.[48] At 2135 cm^{-1} the symmetrical alkynes showed only slight absorption because there was no change in the dipole moment of the molecules and resulted in no vibration in order to obtain absorption. The band at 1634 cm^{-1} which became less intense in CNP-T and may be attributed to the bending mode of absorbed water in carbohydrates and caused by partial reaction of C=O bonds of hemicelluloses.[69] At 1409 cm^{-1} bands correspond to CH_2 bending frequency was observed.[79] The intense band observed at 1017 cm^{-1} is due to C-O-C pyranose ring skeletal vibration and confirmed the presence of higher amount of purified cellulose.[35] At 893 cm^{-1} one small band which was sharper in CNP-T is a typical structure of cellulose I and represents glycosidic deformation of C-H and C-O stretching with ring vibration of O-H bending.[35, 76] and evinced the presence of β-glycosidase linkage between the anhydroglucose units in cellulose.[80]

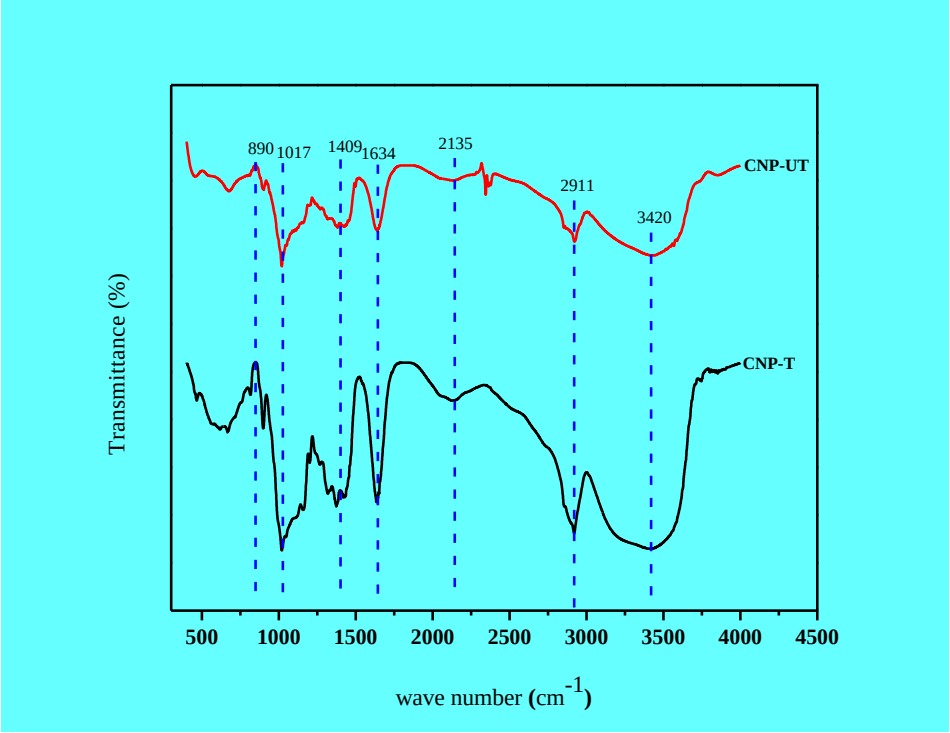

Fig. 4.13 FTIR spectra of CNP-UT and CNP-T

4.7.5 Cross polarization ^{13}C NMR spectroscopy

Solid state high resolution ^{13}C NMR spectra were observed using CP/MAS for CNP-UT and CNP-T nanopaper samples. Figs. 4.14a and 4.14b revealed the characteristic peaks of typical cellulose I which is made up of six signals at C-1, C-4, C-6, C-2, C-3, C-5 and is attributed to anhydroglucose split of supramolecular structure of cellulose into finer cluster.[81] The NMR spectrum confirmed that CNP-UT and CNP-T followed the typical absorbance of cellulose I and is justified to conclude that CNF obtained after chemical and ultrasonic treatments is of high purity cellulose. Native cellulose I is composed of bundles of β-(1, 4) D-glucan polymer chains which exists in the form of fiber. These chains are arranged in supramolecular structure making the chemical structure of cellulose complex. The supramolecular characteristics of these fibrils, such as lateral dimensions, are dependent on the species and isolation process.[82] From Figs. 4.14a and 4.14b it is revealed that there was not much difference in the spectral bands of CNP-UT and CNP-T which evinced that chemical treatment helped in isolation of cellulose effectively. It is further noticeable from the Figures that C-4 and C-6 carbon atoms split into two

sharp bands of lower magnitude field components. The variations in C-4 peak are particularly employed to evaluate crystallinity of cellulose I. The C-4 peak observed at around 88.46-92.73 ppm (CNP-UT) and 87.57-91.76 ppm (CNP-T) are the characteristic of crystalline phase of cellulose Iβ structure.[83] The bands observed at the region of 76.67-79.66 ppm (CNP-UT) and 75.90-78.03 ppm (CNP-T) may be considered as overlapping of C-2, C-3 and C-5 because of the resonance produced from other carbons in pyranose ring.[83] The C-6 spectra at 64.45-67.78 ppm (CNP-UT) and 65.90-68.12 ppm (CNP-T) are similar to C-4 representing crystalline phase and C-1 at 109.57 ppm (CNP-UT) and 108.46ppm (CNP-T) is a Singlet signal attributed to allomorph cellulose Iα.[84] Thus the present study favourably supports that the developed CNP is composed of high purity cellulose with better crystallinity.

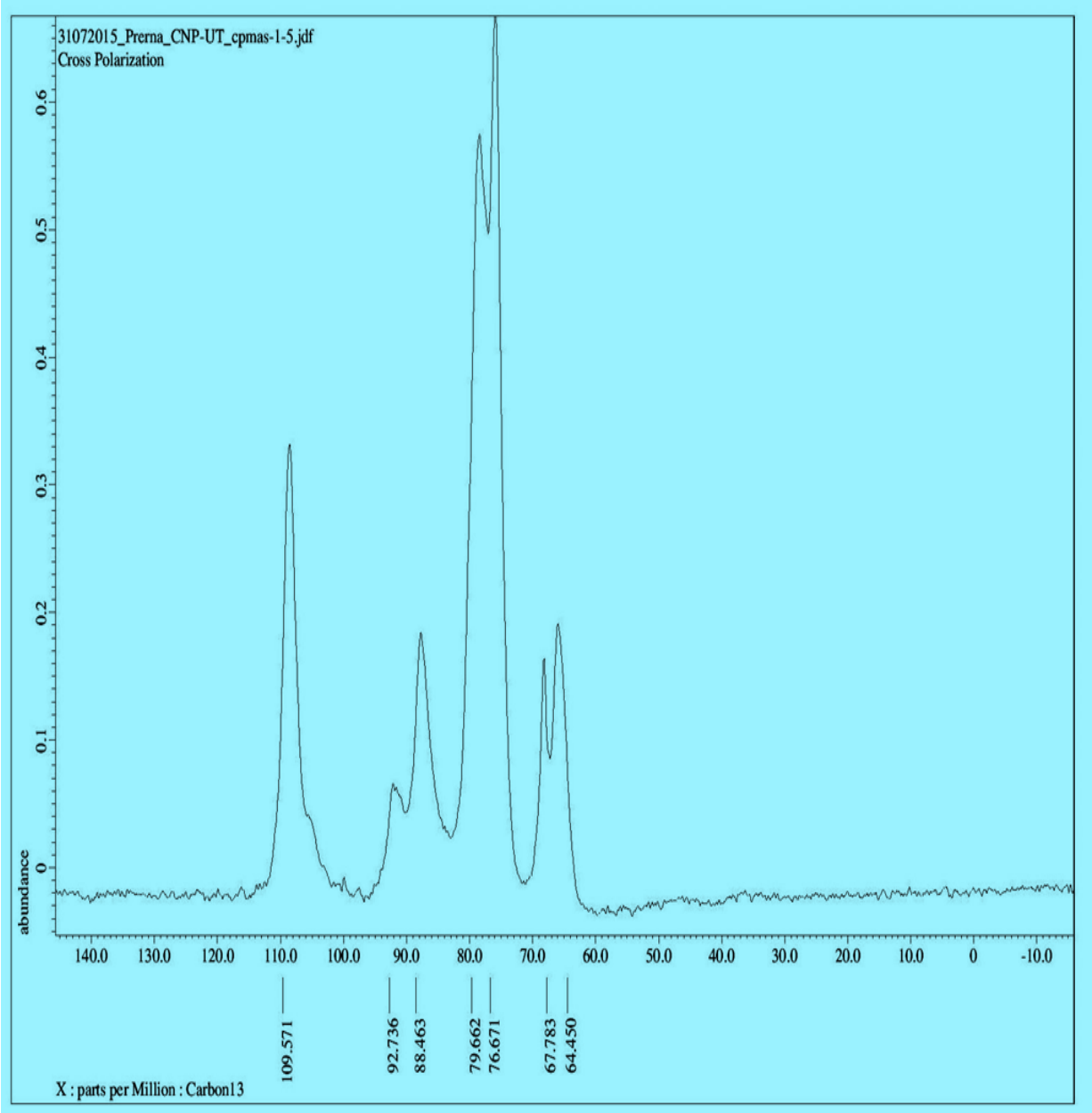

Fig. 4.14a CP/MAS ^{13}C NMR spectra of CNP-UT

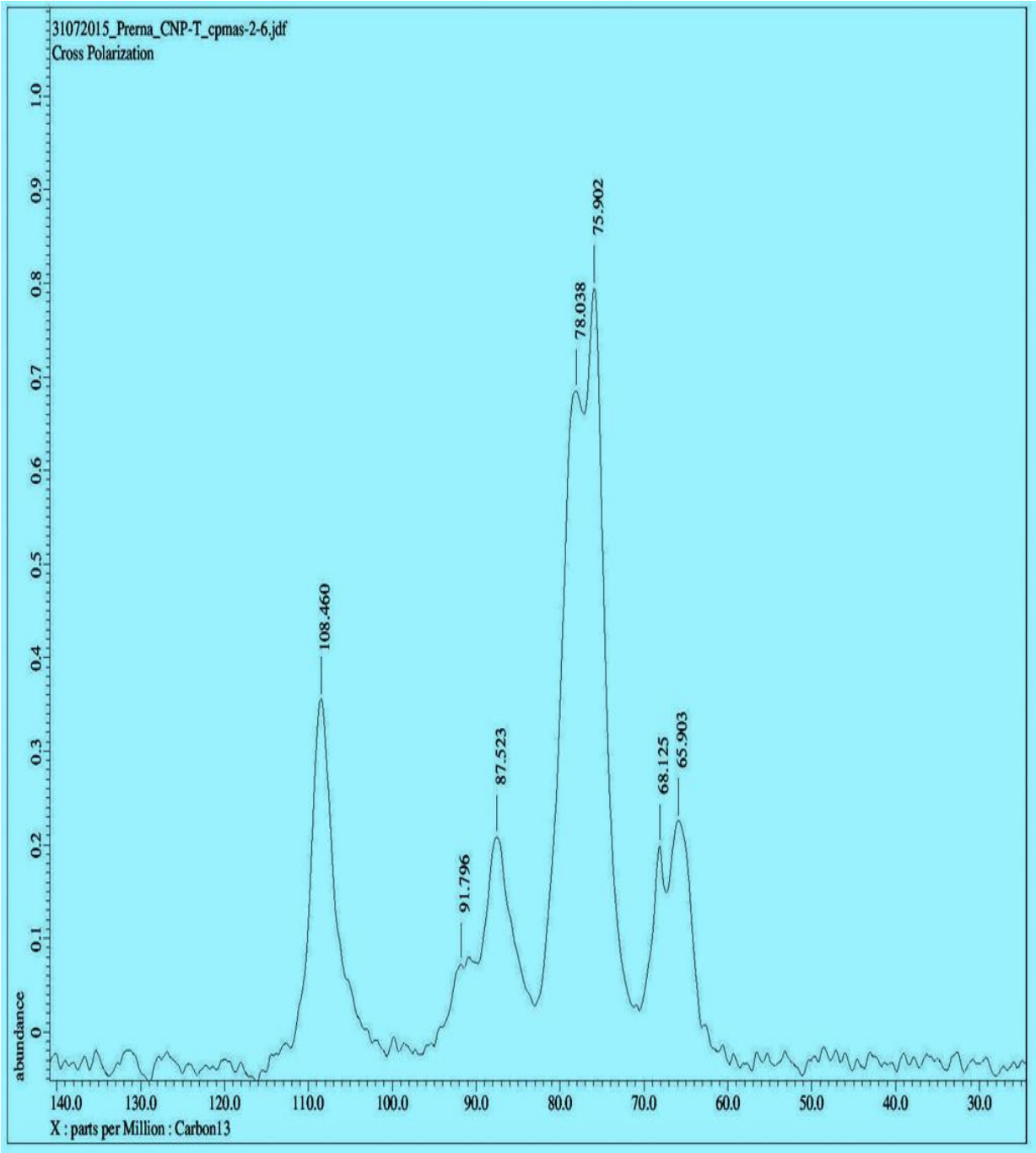

Fig. 4.14b CP/MAS ^{13}C NMR spectra of CNP-T

4.7.6 Thermogravimetric analysis (TGA/DTG)

The thermogravimetric (TGA) and its corresponding derivative thermogravimetric (DTG) analyses of CNP-UT and CNP-T were evaluated to analyze the thermal stability of nanopaper and are illustrated in Figs. 4.15a and 4.15b. The weight loss of both CNP-UT and CNP-T was observed into three steps as revealed in Fig. 4.15a. The initial weight loss started in the region of 21-127^{o}C in CNP-UT and 21-134^{o}C in CNP-T and is attributed to evaporation and removal of absorbed and bound water in nanopaper.[85] The thermal depolymerization of hemicelluloses is attributed by the weight loss in the region of 226-348^{o}C and 239-366^{o}C for CNP-UT and CNP-T respectively. The onset temperature (T_{onset}) was recorded at ~226^{o}C and ~239^{o}C for CNP-UT and CNP-T respectively. The weight loss observed at temperature range of 348-500^{o}C for CNP-UT and 366-510^{o}C for CNP-T are due to pyrolysis of cellulose and amount of fiber's residues which remained after heating to 550^{o}C, indicates the presence of carbonaceous material in culinary banana peel fiber in the nitrogen atmosphere.[25] The higher degradation profile of CNP-T might be attributed to the introduction of hydroxyl groups in the crystallite structure of developed CNP.[86]

Fig. 4.15b illustrates the DTG curves with only one main peak appeared at 311^{o}C for CNP-UT and was shifted to 329^{o}C in case of CNP-T, is the typical degradation point of cellulose molecules.[87] This is due to the degradation of amorpohous compounds present in the cellulose and resulting in char formation. Hence, it can be concluded that improved thermal stability is associated with partial removal of lignin and hemicelluloses and higher crystallinity of the cellulose.[76] The most important application of CNF in the field of nanocomposite is mainly as a reinforcing agent and biocomposite processing, where the processing temperature for thermoplastic polymer rise above 200^{o}C. Hence, the developed CNP bears an excellent thermal stability and will be useful and helpful as a reinforcing material for food packaging. The results of TGA-DTA corroborate with XRD and FT-IR results.

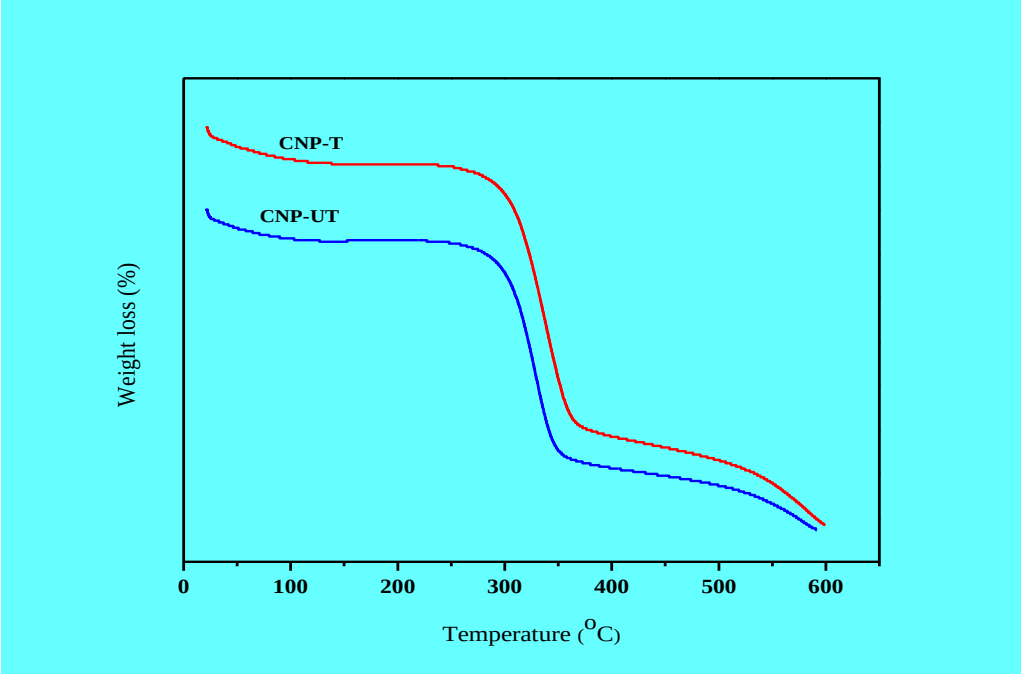

Fig. 4.15a TGA curves of CNP-UT and CNP-T

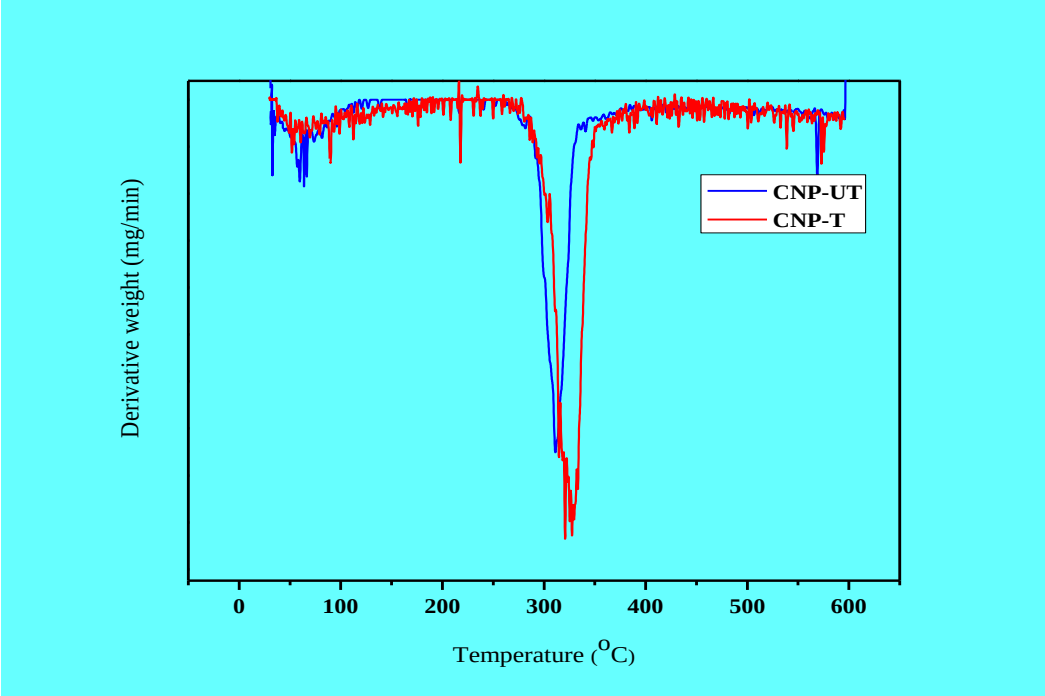

Fig.4.15b DGA curves of CNP-UT and CNP-T

4.7.7 Photoluminescence (PL) and uv-vis spectroscopy

The investigation of light emission was performed using PL in the range of 500-650 nm and observed emission peak at ~614 nm in both CNP-UT and CNP-T with excitation at 490 nm (Fig. 4.16a). The PL spectra of CNP showed that the emission intensity is strongly dependent on photoactive particles in the polymer matrix. In addition, the presence of large number of hydrogen bond between cellulose fibers and crystallization of water associated with CNF may also be confirmed by PL emission curve of CNP.[88] The treatments (chemical and high-intensity ultrasonication) given in order to purify cellulose, might have released additional quantities of protons and hydroxyl ion and improved hydrogen passivation of CNP. The optical property in terms of spectral response of developed CNP was investigated using uv-visible spectrophotometer. The wavelength used was in the range from near ultraviolet (200-400 nm) to the visible light range of 400-700 nm is illustrated in Fig. 4.16b. Both CNP-T and CNP-UT evinced stable tendency towards decreased transmittance with decreasing wavelength. The CNP-T showed higher absorbance rate compared to CNP-UT and may be attributed to smaller particle size of the former.

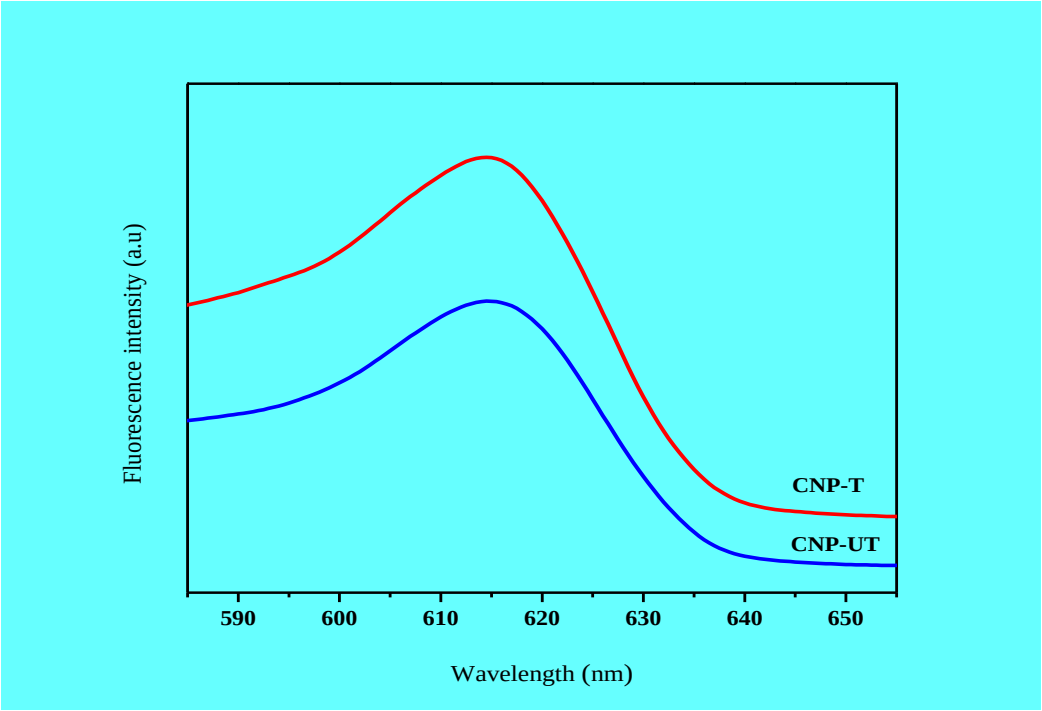

Fig. 4.16a Photoluminescence (PL) emission of CNP-UT and CNP-T

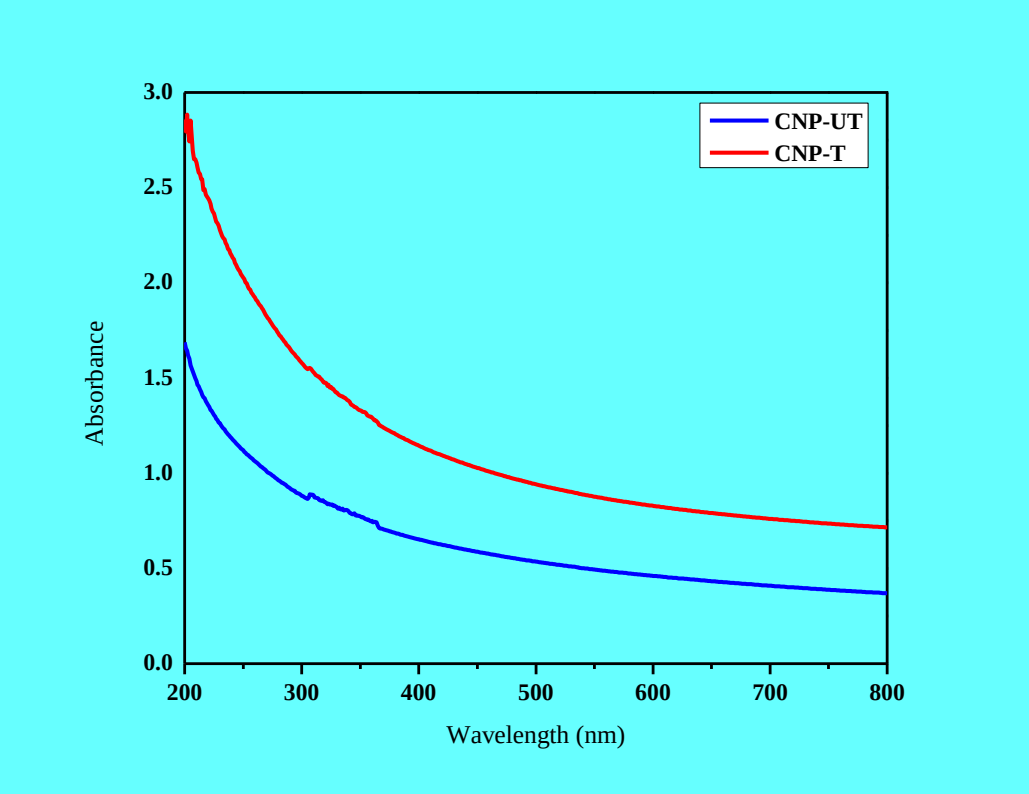

Fig. 4.16b UV-visible spectra of CNP-UT and CNP-T

4.7.8 Mechanical property

The mechanical properties of developed CNP were evaluated in uniaxial tensile test. The stress-strain curve of both CNP-UT and CNP-T are illustrated in Figs. 4.17a and 4.17b and the results are presented in Table 4.4. The CNP-T exhibited excellent tensile property as compared to CNP-UT. The tensile strength of CNP is defined as the maximum tensile force developed in a CNP before its rupture and was measured by applying tensile force to the plane of the CNP which was strong enough to induce a rupture. The tensile strength of CNP-T is higher (1.51 KN/m^2) than CNP-T (0.73 KN/m^2). Tensile energy absorption is the amount of energy per unit surface area (test length × width) of a CNP when it is strained to the maximum tensile force and recorded 2.37 for CNP-UT and 9.00 J/m^2 in case of CNP-T. The maximum compression force per unit area in grams per square meter is the capacity of CNP to withstand loads which was recorded to be extremely satisfactory in CNP-T (755.06 KNm/kg) compared to CNP-UT (376.13 KNm/kg). The strain at break also called as strain-to-failure is a ratio between changes length

and initial length after breakage of CNP which express the capability of a material to resist changes in shape without crack formation. The values of strain at break were recorded 1.52 and 1.10% for CNP-UT and CNP-T respectively. The lower value of strain at break in case of CNP-T is highly desirable in order to have a high thermal stability and it has already been confirmed by TGA/DTG results and the results are of well supportive to conclude that CNP-T possesses good thermal stability. The tensile stiffness index is defined as ratio of the tensile force per unit width to tensile strain within the elastic limit of the tensile-strain relationship which was recorded 1.69 and 6.79 MNm/kg for both CNP-UT and CNP-T respectively. The Young's modulus of CNP-UT was 150.47 MPa and for CNP-T was 326.70 MPa, which is relatively high to be used in reinforcement application. Hence, in terms of a mechanical property the present study revealed that CNP developed from culinary banana peel possesses excellent load bearing characteristics with high tensile strength, Young's modulus and low strain-to-failure ratio.[64]

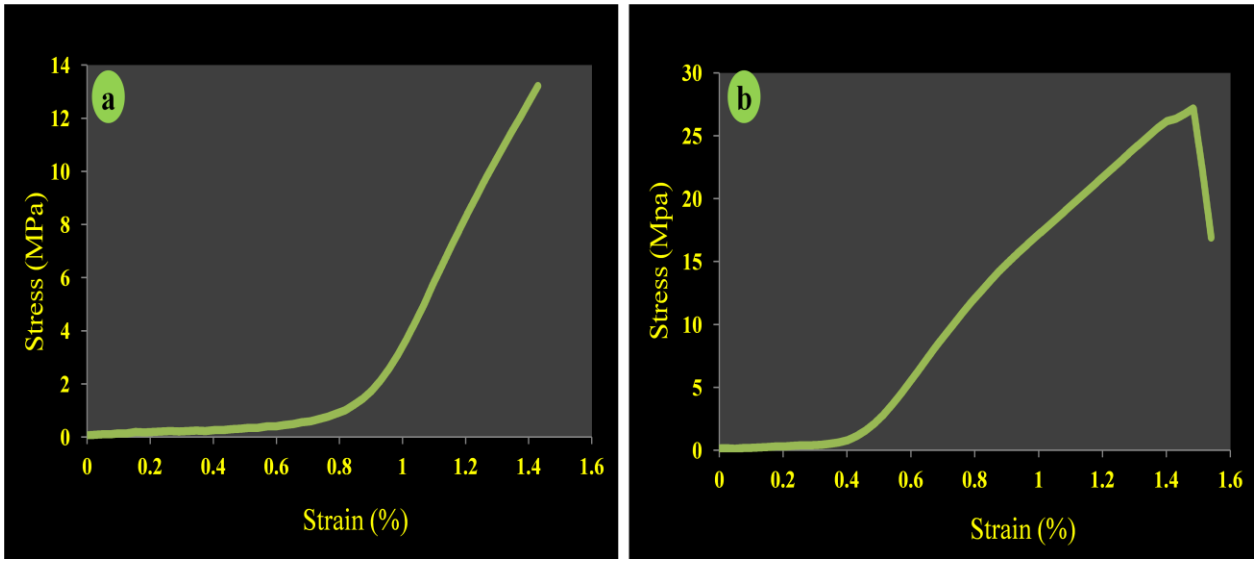

Fig. 4.17 Tensile stress-strain curve of **(a)** CNP-UT and **(b)** CNP-T

Table 4.4 Mechanical properties of CNP

Sample	Tensile strength σ_T^b (KN/m^2)	Tensile energy absorption W_T^b (J/m^2)	Max. compression force σ_T^w (KNm/kg)	Strain at break ε_T (%)	Tensile stiffness E^b (KN/m)	Tensile stiffness index E^w (MNm/kg)	Young's Modulus E (MPa)
CNP-UT	0.73±0.01	2.37±0.06	376.13±3.67	1.52±0.05	3.26±0.03	1.63±0.06	150.47±2.45
CNP-T	1.51±0.02	9.00±0.78	755.06±5.81	1.10±-.11	9.68±1.17	6.79±0.96	326.70±5.64

Values represent mean± SD, n=5

4.7.9 Particle size distribution

The particle size of CNP-UT and CNP-T was characterized in terms of diameter (D), length (L) and aspect ratio (L/D) and are presented in Fig. 4.18 and Table 4.2. The diameter and length of CNF in CNP-UT was 43.76 nm (D) and 1389.65 nm (L) with the aspect ratio of 31.76. On the contrary, it was confirmed that CNP-T is made up of smaller diameter of 10.32 nm and length of 536.07 nm with aspect ratio of 51.94. The credible reason for this is certainly because the high-intensity ultrasonication treatment efficiently facilitated the disintegration and individualization of CNF. The aspect ratio recorded in this study falls in the category of long nanofibers with potential application in biocomposites as reinforcing agent since high aspect ratio favours tension transfer in the in the CNF-matrix interface.[89] The particle size distribution of CNP-UT and CNP-T illustrated in Figure 10 revealed CNP-UT had bimodal distribution with two different length sizes. On the other hand, the CNP-T exhibited unimodal distribution and the peak position of length distribution was comparatively higher than the length distribution of CNP-UT. The treatment of ultrasonication caused the CNF to disintegrate into thinner, shorter and uniform size particles which are desirable for reinforcement application. Our results are in line with the results of Pelissari et al.[35] and Tibolla et al.[38] in case of CNF from banana peel

The zeta potential is the key indicator of surface charge in colloidal suspension and describes the electric potential in solid/liquid interfacial layer of a material in aqueous solution. It also indicates the degree of repulsion of similarly charged particles in dispersion. The zeta potential of CNP-UT and CNP-T measured with the help of dynamic light scattering (DLS) produced a value of -2.6 mV for CNP-UT and 5.4 mV in case of CNP-T. CNP suspension possessed excellent zeta potential and proved to be a promising candidate to use as a reinforcing agent. Nanosize material must have high zeta potential in order to resist aggregation in colloidal suspension and higher electrical stability. Our result of zeta potential values is higher than the value reported by Tibollaet al.[38] Hence, the developed CNP is electrically and thermally stable and could be used competently in polymer matrices as a reinforcing agent.

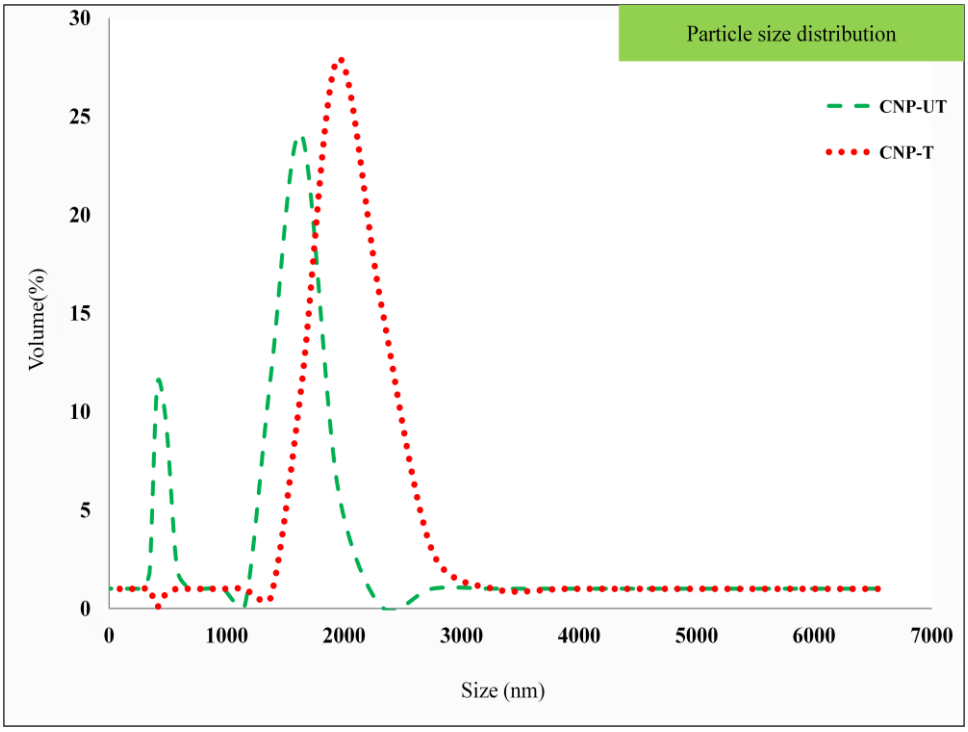

Fig. 4.18 Particle size distribution of CNP-UT and CNP-T

4.8 Conclusions

Cellulose being one of the most predominant natural polymers on earth is currently gaining its importance as a nanostructure material in the form of nanocellulose. In the present study an attempt was made to develop CNP (cellulose nanopaper) from isolated CNF (cellulose nano fiber) of culinary banana peel using chemical and high-intensity ultrasonication treatments. Nanostructure morphology characterized using SEM and TEM confirmed the presence of finer nanofibers in web like structure with partial development of nanotube. XRD showed high crystallinity of CNP-T with individual crystallite size of 2.53 nm. The size of individual crystal of CNP-T is smaller compared to CNP-UT which is due to the ultrasonication treatment given for disintegration of fibers. The bands observed in FT-IR and ^{13}C NMR spectra correlated the typical spectra of cellulose I with higher purity. The developed CNP exhibited high thermal and mechanical stability with maximum degradation temperature in the region of 226-348^{o}C for CNP-UT and 239-366^{o}C for CNP-T with outstanding load bearing characteristic, high tensile strength, high Young's modulus and low strain-to-failure ratio and are excellent properties for

the biomaterial to be used as a reinforcement agent. In addition, higher zeta potential also proved that the developed CNP is electrically and thermally stable. Hence, the developed CNP from culinary banana peel cellulose has credible evidence that it is a potential candidate for nanotechnology application in various areas of packaging including foods with biodegradable and biocompatible as their backbone future.

References

1. Moon, R.J., et al. Cellulose nanomaterials review: structure, properties and nanocomposites. *Chem. Soc. Rev.* **40**, 3941--3994, 2011.
2. Kim, J., & Yun, S. Discovery of cellulose as a smart material. *Macromolecules* **39**(12), 4202-- 4206, 2006.
3. Kadla, J.F., & Gilbert, R.D. Cellulose structure: a review. *Cellul. Chem. Technol.* **34**(3-4), 197--216, 2000.
4. Abraham, E., et al. Extraction of nanocellulose fibrils from lignocellulosic fibres: A novel approach. *Carbohydr. Polym.* **86**(4), 1468--1475, 2011.
5. Chen, W., et al. Individualization of cellulose nanofibers from wood using high-intensity ultrasonication combined with chemical pretreatments. *Carbohydr. Polym.* **83**(4), 1804--1811, 2011.
6. Eichhorn, S.J., Review: current international research into cellulose nanofibres and nanocomposites. *J. Mater. Sci.* **45**(1), 1--33, 2010.
7. Siro, I., & Plackett, D. Microfibrillated cellulose and new nanocomposite materials: A review. *Cellulose* **17**(3), 459--494, 2010.
8. Kalia, S., et al. Cellulose-based bio- and nanocomposites: a review. *Int. J. Polym. Sci.* 2011, 1--35, 2011.
9. Siqueira, G., et al. Cellulose whiskers versus microfibrils: influence of the nature of the nanoparticle and its surface functionalization on the thermal and mechanical properties of nanocomposites. *Biomacromolecules* **10**(2), 425--432, 2009.
10. Rodionova, G., et al. Mechanical and oxygen barrier properties of films prepared from fibrillated dispersions of TEMPO-oxidized Norway spruce and eucalyptus pulps. *Cellulose* **19**(3), 705--711, 2011.
11. Spence, K.L., et al. Water vapor barrier properties of coated and filled microfibrillated cellulose composite films. *BioResour.* **6**(4), 4370--4388, 2011.
12. Fukuzumi, H., et al. Transparent and high gas barrier films of cellulose nanofibers prepared by TEMPO-mediated oxidation. *Biomacromolecules* **10**(1), 162--16, 2009.
13. Iwamoto, S., et al. The effect of hemicelluloses on wood pulp nanofibrillation and nanofiber network characteristics. *Biomacromolecules* **9**(3), 1022--1026, 2008.

14. Yoo, S., & Hsieh, J. S. Enzyme-assisted preparation of fibrillated cellulose fibers and its effect on physical and mechanical properties of paper sheet composites. *Ind. Eng. Chem. Res.* **49**(5), 2161--2168, 2010.
15. Henriksson, M., et al. Cellulose nanopaper structures of high toughness. *Biomacromolecules* **9**(6), 1579--1585, 2008.
16. Cherian, B.M., et al. Cellulose nanocomposites with nanofibres isolated from pineapple leaf fibres for medical applications. *Carbohydr. Polym.* **86**(4), 1790--1798, 2011.
17. Czaja, W.K., et al. The future prospects of microbial cellulose in biomedical applications. *Biomacromolecules* **8**(1), 1--12, 2007.
18. Turbak, A.F., Snyder, F. W., & Sandberg, K. R. Microfibrillated cellulose, a new cellulose product: properties, uses, and commercial potential. In: Sarko A ed., Proceedings of the Ninth Cellulose Conference, Applied Polymer Symposium, Wiley, New York, 1983, 815--827.
19. Abe, K., et al. Obtaining cellulose nanofibers with a uniform width of 15 nm from wood. *Biomacromolecules* **8**(10), 3276--3278, 2007.
20. de Morais, T.E., et al. Cellulose nanofibers from white and naturally colored cotton fibers. *Cellulose* **17**(3), 595--606, 2010.
21. Dufresne, A., et al. Cellulose microfibrils from potato tuber cells: Processing and characterization of starch-cellulose microfibril composites. *J. Appl. Polym. Sci.* **76**(14), 2080--2092, 2000.
22. Habibi, Y., et al. Morphological and structural study of seed pericarp of *Opuntia ficus-indica* prickly pear fruits. *Carbohydr. Polym.* **72**(1), 102--112, 2008.
23. Rondeau-Mouro, C., et al. Structural features and potential texturising properties of lemon and maize cellulose microfibrils. *Carbohydr. Polym.* **53**(3), 241--252, 2003.
24. Wang, B., & Sain, M. Isolation of nanofibers from soybean source and their reinforcing capability on synthetic polymers. *Compos. Sci. Technol.* **67**(11-12), 2521--2527, 2007.
25. Alemdar, A., & Sain, M. Isolation and characterization of nanofibers from agricultural residues -wheat straw and soy hulls. *Bioresour. Technol.* **99**(6), 1664--1671, 2008a.
26. Rosa, M.F., et al. Cellulose nanowhiskers from coconut husk fibers: Effect of preparation conditions on their thermal and morphological behavior. *Carbohydr. Polym.* **81**(1), 83--92, 2010.

27. Li, R., et al. Cellulose whiskers extracted from mulberry: A novel biomass production, carbohydrate polymers. *Carbohydr. Polym.* **76**(1), 94--99, 2009.
28. Cherian, B.M., et al. Isolation of nanocellulose from pineapple leaf fibres by steam explosion. *Carbohydr. Polym.* **81**(3), 720--725, 2010.
29. Zuluaga, R., et al. Cellulose microfibrils from banana rachis: Effect of alkaline treatments on structural and morphological features. *Carbohydr. Polym.* **76**(1), 51--59, 2009.
30. Chen, Y., et al. Bionanocomposites based on pea starch and cellulose nanowhiskers hydrolyzed from pea hull fibre: Effect of hydrolysis time. *Carbohydr. Polym.* **76**(4), 607--615, 2009.
31. Dinand, E., et al. Suspensions of cellulose microfibrils from sugar beet pulp. *Food Hydrocolloids* **13**(3), 275--283, 1999.
32. Chakraborty, A., et al. Reinforcing potential of wood pulp-derived microfibres in a PVA matrix. *Holzforschung* **60**(1), 53--58, 2006.
33. Abe, K., & Yano, H. Comparison of the characteristics of cellulose microfibril aggregates isolated from fiber and parenchyma cells of Moso bamboo (*Phyllostachys pubescens*). *Cellulose* **17**(2), 271--277, 2010.
34. Abe, K., et al. High-strength nanocomposite based on fibrillated chemi-thermomechanical pulp. *Compos. Sci. Technol.* **69**(14), 2434--2437, 2009.
35. Pelissari, M.F., et al. Isolation and characterization of cellulose nanofibers from banana peels. *Cellulose* **21**(1), 417--432, 2014.
36. Liu, H., et al. Fabrication and properties of transparent polymethylmethacrylate/cellulose nanocrystals composites. *Bioresour. Technol.* **101**(14), 5685--5692, 2010.
37. Elazzouzi-Hafraoui, S., et al. The shape and size distribution of crystalline nanoparticles prepared by acid hydrolysis of native cellulose. *Biomacromolecules* **9**(1), 57--65, 2008.
38. Tibolla, H., et al. Cellulose nanofibers produced from banana peel by chemical and enzymatic treatment. *LWT--Food Sci. Technol.* **59**(2), 1311--1318, 2014.
39. Paakko, M., et al. Enzymatic hydrolysis combined with mechanical shearing and high-pressure homogenization for nanoscale cellulose fibrils and strong gels. *Biomacromolecules* **8**(6), 1934--1941, 2007.
40. Cheng, Q., et al. Novel process for isolating fibrils from cellulose fibers by high-intensity ultrasonication. II. Fibril characterization. *J. Appl. Polym. Sci.* **115**(5), 2756--2762, 2010

41. Cheng, Q., et al. Poly (vinyl alcohol) nanocomposites reinforced with cellulose fibrils isolated by high intensity ultrasonication. *Compos Part A: Appl. Sci. Manufac.* **40**(2), 218--224, 2009.
42. Wang, S., & Cheng, Q. A novel process to isolate fibrils from cellulose fibers by high-intensity ultrasonication, Part 1: Process optimization. *J. Appl. Polym. Sci.* **113**(2), 1270--1275, 2009.
43. Tischer, P.C.S.F., et al. Nanostructural reorganization of bacterial cellulose by ultrasonic treatment. *Biomacromolecules* **11**(5), 1217--1224, 2010.
44. Emaga, T.H., et al. Effects of the stage of maturation and varieties on the chemical composition of banana and plantain peels. *Food Chem.* **103**(2), 590--600, 2007.
45. Dufresne, A., et al. Mechanical behavior of sheets prepared from sugar beet cellulose microfibrils. *J. Appl. Polym. Sci.* **64**(6), 1185--1194, 1997.
46. Somerville, C., et al. Toward a systems approach to understanding plant cell walls. *Sci.* **306**(5705), 2206--2211, 2004.
47. Sao, K., et al. Infrared spectra of alkali treated degummed Ramie. *Text. Res. J.* **57**(7), 407--414, 1987.
48. Xu, F., et al. Comparative study of water-soluble and alkali-soluble hemicelluloses from perennial ryegrass leaves (*Lolium peree*). *Carbohydr. Polym.* **67**(1), 56--65, 2007a.
49. Xu, F., et al. Fractionation and characterization of chlorophyll and lignin from de-juiced Italian ryegrass (*Lolium multifolrum*) and timothy grass (*Phleum pratense*). *Process Biochem.* **42**(5), 913--918, 2007b.
50. Sun, J. X., et al. Physicochemical and thermal characterization of cellulose from barley straw. *Polym. Degrad. Stab.* **88**(3), 521--531, 2005.
51. Wang, B., et al. Study of structural morphology of hemp fiber from the micro to the nanoscale. *Appl. Compos. Mater.* **14**(2), 89--103, 2007.
52. Xiao, B., et al. Chemical, structural, and thermal characterization of alkali-soluble lignins and hemicelluloses, and cellulose from maize stems, rye straw, and rice straw. *Polym. Degrad. Stab.* **74**(2), 307--319, 2001.
53. Alemdar, A., & Sain, M. Biocomposites from wheat straw nanofibers: Morphology, thermal and mechanical properties. *Compos. Sci. Technol.* **68**(2), 557--565, 2008b.

54. Ghaderi, M., et al. All-cellulose nanocomposite film made from bagasse cellulose nanofibers for food packaging application. *Carbohydr. Polym.* **104**(15), 59--65, 2014.
55. Deepa, B., et al. Structure, morphology and thermal characteristics of banana nano fibers obtained by steam explosion. *Bioresour. Technol.* **102**(2), 1988--1997, 2011.
56. Roman, M., & Winter, W.T. Effect of sulfate groups from sulfuric acid hydrolysis on the thermal degradation behavior of bacterial cellulose. *Biomacromolecules* **5**(5), 1671--1677, 2004.
57. Lin, N., & Dufresne, A., Nanocellulose in biomedicine: Current status and future prospect. *Eur. Polym. J.* **59**, 302--325, 2014.
58. Kontturi, E., et al. Cellulose-model films and the fundamental approach. *Chem. Soc. Rev.* **35**(12), 1287--1304, 2006.
59. Lee, K.-Y., et al. On the use of nanocellulose as reinforcement in polymer matrix composites. *Compos. Sci. Technol.* **105**, 15--27, 2014.
60. Irimia-Vladu, M. ‘‘Green’’ electronics: biodegradable and biocompatible materials and devices for sustainable future. *Chem. Soc. Rev.* **43**(2), 588--610, 2014.
61. Sehaqui, H., et al. Wood cellulose biocomposites with fibrous structures at micro-and nanoscale. *Compos. Sci. Technol.* **71**(3), 382--387, 2011a.
62. Hu, L., et al. Transparent and conductive paper from nanocellulose fibers. *Energy Environ. Sci.* **6**(2), 513--518, 2013.
63. Sehaqui, H., et al. Strong and tough cellulose nanopaper with high specific surface area and porosity. *Biomacromolecules* **12**(10), 3638--3644, 2011b.
64. Sehaqui, H., et al. Cellulose nanofiber orientation in nanopaper and nanocomposites by cold drawing. *ACS Appl. Mater. Interfaces* **4**(2), 1043--1049, 2012.
65. Sehaqui, H., et al. Hydrophobic cellulose nanopaper through a mild esterification procedure. *Cellulose* **21**(1), 367--382, 2014.
66. Sehaqui, H., et al. Fast preparation procedure for large, flat cellulose and cellulose/inorganic nanopaper structures. *Biomacromolecules* **11**(9), 2195--2198, 2010.
67. Ho, T.T., et al. Composites of cationic nanofibrillated cellulose and layered silicates: water vapor barrier and mechanical properties. *ACS Appl. Mater. Interfaces* **4**(9), 4832--4840, 2012.

68. Osterberg, M., et al. A fast method to produce strong NFC films as a platform for barrier and functional materials. *ACS Appl. Mater. Interfaces* **5**(11), 4640-4647, 2013.
69. Urruzola, I., et al. Nanopaper from almond (*Prunus dulcis*) shell. *Cellulose* **21**(3), 1619--1629, 2014.
70. Sugimoto, H., et al. Enhanced photoluminescence of Si nanocrystals-doped cellulose nanofibers by plasmonic light scattering. *Appl. Phys. Lett.* **107**, 041111--4, 2015.
71. Kalita, E., et al. High quality fluorescent cellulose nanofibers from endemic rice husk: Isolation and characterization. *Carbohydr. Polym.* **122**, 308--313, 2015.
72. Salajkova, M., et al. Tough nanopaper structures based on cellulose nanofibers and carbon nanotubes. *Compos. Sci.Technol.* **87**, 103--110, 2013.
73. Gonzalez, R.J., et al. Long-length titania nanotubes obtained by high-voltage anodization and high-intensity ultrasonication for superior capacity electrode. *J. Phys. Chem.* **116**(38), 20182--20190, 2012.
74. Yamada, T., et al. Synthesis of carbon nanotube/silver nanocomposites by ultrasonication. *Mater. Transactions* **51**(10), 1769 --1772, 2010.
75. Johar, N., et al. Extraction, preparation and characterization of cellulose fibres and nanocrystals from rice husk. *Ind. Crops Prod.* **37**(1), 93--99, 2012.
76. Xu, C., et al. Isolation and properties of cellulose nanofibrils from coconut palm petioles by different mechanical process. *PLoS One* **10**(4), 1--11, 2015.
77. Mwaikambo, L.Y., & Ansell, M.P. Mechanical properties of alkali treated plant fibres and their potential as reinforcement materials. I. Hemp fibres. *J. Mater. Sci.* **41**(8), 2483--2496, 2006.
78. de Lima, M.M.S., & Borsali R. Rodlike cellulose microcrystals: Structure, properties, and applications. *Macromol. Rapid Commun.* **25**(7), 771--787, 2004.
79. Sun, J.X., et al. Isolation and characterization of cellulose from sugarcane bagasse. *Polym. Degrad. Stab.* **84**(2), 331--339, 2004.
80. Buschle-Diller, G., et al. Physicochemical properties of chemically and enzymatically modified cellulosic surfaces. *Colloids Surfaces A Physicochem. Eng. Aspects* **260**(1-3), 63--70, 2005.
81. Larson, P.T., et al. CP/MAS ^{13}C-NMR spectroscopy applied to structure and interaction studies on cellulose I. *Solid State Nucl. Magn. Reson.* **15**(1), 31--40, 1999.

82. Peciulyte, A., et al. Impact of the supramolecular structure of cellulose on the efficiency of enzymatic hydrolysis. *Biotechnol. Biofuels* **8**(56) 1--13, 2015.
83. Marino, M., et al. Enhanced materials from nature: nanocellulose from citrus waste. *Molecules* **20**(4), 5908--5923, 2015.
84. VanderHart, D.L., & Atalla, R.H., Studies of microstructure in native celluloses using solid-state carbon-13 NMR. *Macromolecules* **17**(8), 1465--1472, 1984.
85. Yousefi, H., et al. Comparative study of paper and nanopaper properties prepared from bacterial cellulose nanofibers and fibers/ground cellulose nanofibers of canola straw. *Ind. Crops Prod.* **43**, 732--737, 2013.
86. Kaushik, A., & Singh, M., Isolation and characterization of cellulose nanofibrils from wheat straw using steam explosion coupled with high shear homogenization. *Carbohydr. Res.* **346**(1), 76--85, 2011.
87. Sun, X., et al. Comparison of highly transparent all-cellulose nanopaper prepared using sulfuric acid and TEMPO-mediated oxidation methods. *Cellulose* **22**(2), 1123--1133, 2015.
88. Pikulev, V., et al. Luminescence properties of silicon-cellulose nanocomposites. *Nanoscale Res. Lett.* **7**(426), 1--6, 2012.
89. George, J., et al. Bacterial cellulose nanocrystals exhibiting high thermal stability and their polymer nanocomposites. *Int. J. Biol. Macromol.* **48**(1), 50--57, 2011.